https://doi.org/10.31436/iiumej.v27i1.3720

Development of Electric Fence Fault Sensing and Monitoring System with LoRaWAN IoT

M. SYARIFUDDIN M. SUFIAN[1*], HISHAM MOHAMAD[1], M. AZMAN ZAKARIYA[2], AIZAT AKMAL A. MOHAMAD BEDDELEE[1], SALMAN SAABAN[3], M. FADLLI A. YAZI[3]

[1]Civil & Environmental Engineering Department,
Universiti Teknologi PETRONAS, 32610 Seri Iskandar, Perak Malaysia
[2]Electrical & Electronics Engineering Department,
Universiti Teknologi PETRONAS, 32610 Seri Iskandar, Perak Malaysia
[3]Department of Wildlife and National Parks Peninsular Malaysia (PERHILITAN),
56100 Kuala Lumpur, Malaysia

**Corresponding author: syarifuddin_16001417@utp.edu.my*

(Received: 13 May 2025; Accepted: 1 October 2025; Published online: 12 January 2026)

ABSTRACT: The persistent challenge of Human-Elephant Conflict (HEC) in regions like Malaysia necessitates robust and efficient mitigation strategies. Electric fences are effective but often face maintenance inefficiencies due to delayed fault detection. This study presents a smart electric fence monitoring system designed for real-time fault diagnosis and localisation. The system employs IoT-enabled in-place sensor nodes comprising 10 kV voltage sensors, short-circuit detection sensors, and 3-axis gyroscope sensors. Sensor data is transmitted via a LoRaWAN network, selected for its long-range, low-power characteristics, which are well-suited to rural, low-bandwidth environments where electric fences are typically deployed. Field validation of a 50 m, 10 kV, 6 A electric fence segment achieved 100% voltage and short-circuit detection rates and 99.91% gyroscope tilt accuracy. Reliable data transmission was maintained up to 1.3 km, with an RSSI of -110 dBm, in campus environments with concrete obstructions. Supplementary testing at the same positions using antennas at increased height yielded an RSSI of -79 dBm, with a 41 dB link margin, highlighting the potential for range scaling in future work. The system has so far been validated on a short 50 m electric fence segment with a practical LoRaWAN range of 1.3 km under campus conditions, indicating the need for further optimisation and field-scale trials. The system provides a practical solution for the Department of Wildlife and National Parks Peninsular Malaysia (PERHILITAN), with direct application to their Sistem Pagar Elektrik Gajah (SPEG) for HEC mitigation. Beyond this application, the approach demonstrates potential for future use of IoT-based Structural Health Monitoring (SHM) concepts in resource-constrained rural infrastructures.

ABSTRAK: Cabaran berterusan Konflik Manusia-Gajah (HEC) di kawasan seperti Malaysia memerlukan strategi mitigasi yang kukuh dan berkesan. Pagar elektrik berkesan dalam menangani konflik ini, tetapi sering berhadapan masalah penyelenggaraan akibat kelewatan pengesanan kerosakan pada pagar. Kajian ini membentangkan satu sistem pemantauan pagar elektrik pintar yang direka bagi mengdiagnosis penentuan lokasi kerosakan secara masa nyata. Sistem ini menggunakan nod sensor dengan keupayaan internet benda terdiri daripada sensor voltan 10 kV, sensor pengesan litar pintas, dan sensor giroskop. Data sensor dihantar melalui rangkaian LoRaWAN, yang dipilih atas dasar rangkaian jarak jauh dan penggunaan tenaga minimal. Ciri-ciri ini dianggap bersesuaian bagi persekitaran luar bandar di mana pagar elektrik biasanya terpasang, kerana kawasan ini seringkali tidak mendapat rangkaian telekomunikasi komersial. Ujian lapangan pada segmen pagar elektrik sepanjang 50 m, 10 kV 6 A telah berjaya mengesan voltan dan litar pintas dengan ketepatan 100%, manakala sensor giroskop pula mampu mengesan kecondongan pada kadar 99.91%. Penghantaran data

https://doi.org/10.31436/iiumej.v27i1.3720

daripada sensor pula berjaya mencapai jarak maximum 1.3 km dengan RSSI -110 dBm dalam persekitaran kampus (yang mempunyai pelbagai halangan konkrit). Ujian sampingan penghantaran data yang dilaksanakan menggunakan antena berkedudukan tinggi pada lokasi dan jarak yang sama pula menunjukkan RSSI -79 dBm dengan margin pautan 41 dB. Ini menunjukkan potensi peningkatan jarak penghantaran data bagi kajian seterusnya. Pada masa ini, sistem ini telah disahkan kepenggunaanya bagi segmen pagar elektrik pendek dengan kepanjangan 50 m, manakala penghantaran data secara berkesan dihadkan pada 1.3 km dalam persekitaran kampus. Had ini menunjukkan, wujud keperluan bagi kerja-kerja penambah baikan untuk meningkatkan kadar keberkesanan melalui ujian berskala besar di lapangan pada masa hadapan. Sistem ini menyediakan penyelesaian kejuruteraan yang praktikal untuk Jabatan Perlindungan Hidupan Liar dan Taman Negara Semenanjung Malaysia (PERHILITAN), dengan aplikasi langsung pada Sistem Pagar Elektrik Gajah (SPEG) bagi mitigasi HEC. Kajian ini juga menunjukkan potensi bagi penggunaan konsep Pemantauan Kesihatan Struktur (SHM) berasaskan IoT pada masa hadapan dalam infrastruktur luar bandar.

KEYWORDS: *LoRaWAN, Electric Fence, RFM95, STM32F103C8T6, In-Placed Sensors.*

1. INTRODUCTION

Human-Elephant Conflict (HEC) poses a critical challenge due to unpredictable elephant incursions into human settlements, resulting in substantial socioeconomic and ecological impacts. In Peninsular Malaysia, HEC has caused annual crop losses of approximately RM 2.96 million across 11,460 acres of plantations, while mitigation and repair costs have exceeded RM 3.59 million over five years [1]. Between 2008 and 2019, at least 12 human fatalities were recorded [2], alongside heightened risks to elephant populations, with five elephants killed in retaliatory incidents and four in vehicle collisions since 2018 [3].

To address these conflicts, governments have implemented various deterrent measures, with electric fences emerging as the primary solution. The Malaysian government alone has invested more than RM 6 million in nationwide electric fence infrastructure [4,5]. However, these capital expenditures are compounded by substantial recurring costs. A single energiser station, covering roughly 4 km of fence, requires RM 19,200-RM 28,800 annually for routine maintenance, including voltage inspections, system checks, and vegetation management [6]. Improving fault detection and maintenance efficiency is, therefore, critical to sustaining this investment.

Electric fences are designed to be highly effective physical and psychological barriers against elephant intrusions [7-9]. A typical system consists of an energiser (high-voltage transformer), power sources (batteries and solar panels), conductive wiring, grounding, and structural supports. In Malaysia, such systems have demonstrated approximately 80% effectiveness in protecting oil palm and rubber plantations [10]. According to PERHILITAN's guidelines, electric fences must deliver high-voltage pulses of 6-10 kV at an impulse energy of 12 J, with a maximum repetition frequency of 1 Hz [6].

The architecture of an electric fence system generally adopts one of two wiring configurations. As illustrated in Figure 1, electric fence cables can be connected using an all-live wire system or a ground-return wire system, depending on site-specific environmental conditions [11]. In humid regions where soil conductivity is adequate, all-live systems are commonly employed. Conversely, in areas with low ground conductivity, ground-return configurations are preferred to ensure that electric pulses are delivered effectively through simultaneous contact with live and ground wires.

https://doi.org/10.31436/iiumej.v27i1.3720

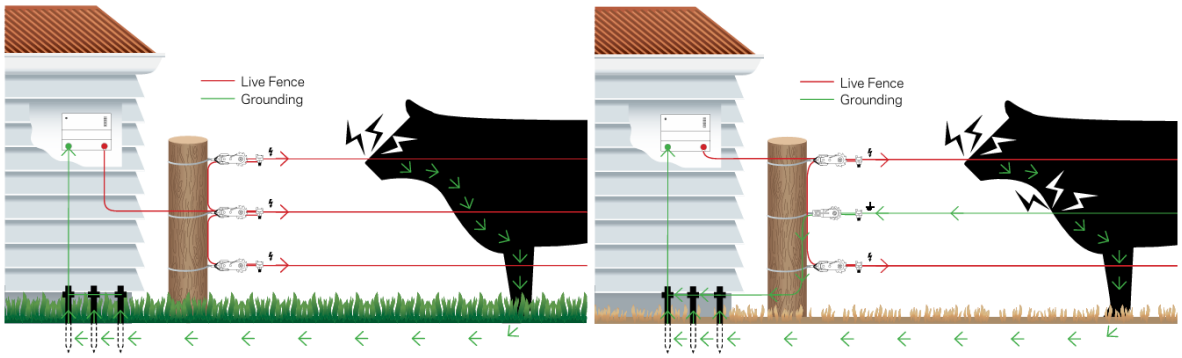

(a) All-live cable wire system. (b) Ground return wire system

Figure 1. Electric fence system wire connection configurations [11].

In Malaysia, the elephant electric fence system has been standardised through the implementation of the Sistem Pagar Elektrik Gajah (SPEG), developed by the Department of Wildlife and National Parks Peninsular Malaysia (PERHILITAN) as a strategic measure to mitigate Human-Elephant Conflict. The SPEG design specifies a multi-wire configuration with fences 1.5-1.8 m high. The fence incorporates three to five high-tensile galvanised steel wires, connected in parallel and spaced at 30-60 cm gaps. To prevent short circuits, the cables are supported by Acrylonitrile Butadiene Styrene (ABS) insulators mounted on galvanised steel, wood, or PVC poles, with support poles spaced 5-10 m apart [6]. The Pel 412i Unigizer™ is the standard energiser used in the SPEG to power 4 km of fence, commonly referred to as a "bay." The SPEG uses the all-live wire system architecture, with grounding achieved through the installation of at least three galvanised rods, each 1.5-2 m long and spaced at 3 m intervals [6].

Despite these sophisticated installations, operational effectiveness is constrained by technical and logistical challenges. Fences remain vulnerable to elephant-induced damage at poles and supports, while fallen trees and vegetation frequently disrupt integrity [12]. These issues cause voltage drops that compromise deterrent capacity. Additionally, maintaining fences across vast rural areas requires intensive manual inspections, and current technologies offer limited capacity for rapid, accurate fault detection in remote environments.

This research addresses these challenges by developing a remote electric fence monitoring system to improve maintenance efficiency and system reliability. The proposed solution integrates custom-developed sensors with a robust Long-Range Wide Area Network (LoRaWAN) communication infrastructure, enabling real-time voltage monitoring, fault localisation, and structural integrity assessment. Conducted in collaboration with the Department of Wildlife and National Parks Peninsular Malaysia (PERHILITAN), the system is designed to meet key requirements, namely detecting voltage drops, pinpointing short-circuit locations, monitoring leaning poles, operating at low power, and supporting easy plug-and-play deployment. This initiative directly enhances the effectiveness of electric fences as a sustainable HEC mitigation strategy.

2. LITERATURE REVIEW & RELATED WORKS

Electric fences are widely utilised to mitigate human-elephant conflict (HEC). However, their operational reliability is frequently compromised by damage and malfunctions, resulting in system faults. The faults disrupting the fence's intended function include wire breaks, connection failures, grounding issues, or any event that reduces the system's effectiveness in deterring elephants. Timely detection and rectification of these faults are crucial for

https://doi.org/10.31436/iiumej.v27i1.3720

maintaining the integrity and efficacy of the electric fence system. To develop a monitoring system for an electric fence, findings from previous research have been studied. The review encompasses electric fence monitoring mechanisms and suitable types of communication systems for the application.

2.1. Electric Fence Monitoring Technologies

Current fault detection technologies can be broadly categorised into patrol control devices, in-place sensors, and functional analysis. This study focuses on developing in-place sensor systems, recognised for their intuitive and passive monitoring capabilities. Several studies, including Tennakoon et al. [12], Al-Bahadly and Simpson [13], Ali et al. [14], and Yunus and Zainal [15], have examined various electric fence monitoring systems to address these challenges. A summary of these studies is presented in Table 1.

In a study, Tennakoon et al. [12] developed a system that detects and localizes wire breakage in a ground-return electric fence system connected in series. This method uses two sensor systems: one for wire-breakage detection and another for open-circuit detection on the electric fence. The sensors were mounted on the fence in a wired assembly, using the fence cables as a communication medium. The proposed system utilises two pulse generators, each for generating a high voltage (10kV deterrent) and a communication step voltage (fault detection). The use of these pulse generators is accompanied by switching components, detectors, and other devices, as depicted in Figure 2.

The fence controller manages the switching function between the fence pulse generator and the communication pulse generator. This enables the application of different pulses (high and low voltages) on the electric fence cables. The communication pulse generator supplies unique PWM pulses and requires only a single unit per fence [12]. The first system, wire breakage detection, comprises the detector, detectors 1 and 2, and the end node. The second system for locating the breakage comprises nodes 1, 2, and 3, along with their relays. The controller detector has two functions: to detect wire breakages and the sensor IDs of the nodes (1, 2, and 3). It is connected to the main system, which comprises a single-board computer (Raspberry Pi) for signal processing. Wires 1 and 3 are connected to the fence controller as live cables, while wire 2 is connected as a ground cable.

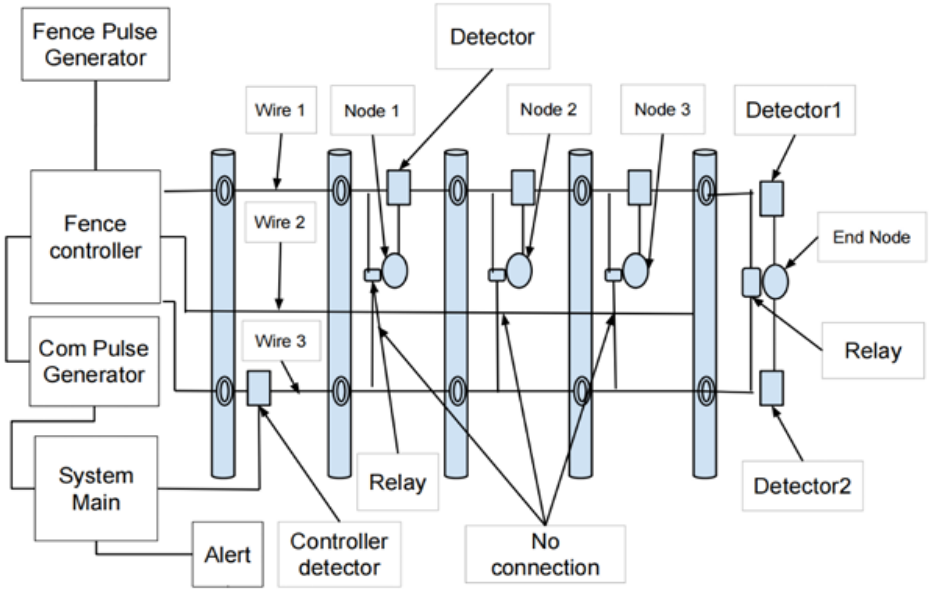

Figure 2. System design for detection and communication [12].

https://doi.org/10.31436/iiumej.v27i1.3720

The system uses a fixed 15-minute interval to monitor the health of an electric fence. The wire breakage detector system begins by closing the relay at the end node and switching wire 3 from a live connection to a ground connection. This creates a complete high-voltage loop between wires 1 and 3 [12]. The controller detector is equipped with a voltage detector that detects the presence of a high-voltage pulse, indicating wire breakage. If no pulse is detected, the wire breakage locator system is triggered.

The breakage locator process begins when the fence controller switches from the fence pulse generator to the communication pulse generator. Concurrently, the nodes (1, 2, 3) and the end node close the relays along the fence. This allows the communication pulse to flow through each sensor node back to the controller detector. Once each sensor detects a pulse, it returns the signal with its unique binary ID for detection by the controller. The "system main" then determines the location of the breakage based on the signals returned by the sensor nodes. For any breakages, the alert is used to notify users of the faulty condition [12].

While this approach accurately detects wire breaks in an electric fence system, it is limited to wire breaks and does not detect other faults, such as voltage drops or short circuits. It is also applicable only to a series-connected ground-return electric fence system, whereas the SPEG system uses a parallel all-live electric fence system. Due to the absence of a dedicated return conductor and the parallel distribution of high-voltage output across multiple live wires in SPEG, Tennakoon's pulse-injection method cannot establish the closed diagnostic loop on which it relies. As a result, the signal attenuation and path uncertainty inherent to SPEG preclude the reliable operation of Tennakoon's system without substantial redesign. This study, however, inspired the adaptation of a 12V DC supply that operates in parallel with the electric fence energiser's 10kV pulse for a short-circuit locator system. It is also considered a simpler approach than a complex PWM system that utilises multiple components.

Al-Bahadly and Simpson [13] proposed a contactless fault detection method that uses an antenna and an oscilloscope to measure the Electromagnetic Field (EMF) generated by the high-voltage fence line. The technique uses a coil with 50 turns connected to an oscilloscope to measure the miniature voltage generated by the induced current via its EMF, as illustrated in Figure 3. The developed EMF sensor (antenna) was tested by shorting the middle of a 100 m electric fence cable. The test uses a single cable all-live electric fence design, and the developed antenna successfully detected voltage and current changes under normal and fault conditions at distances of up to 1 m from the wire.

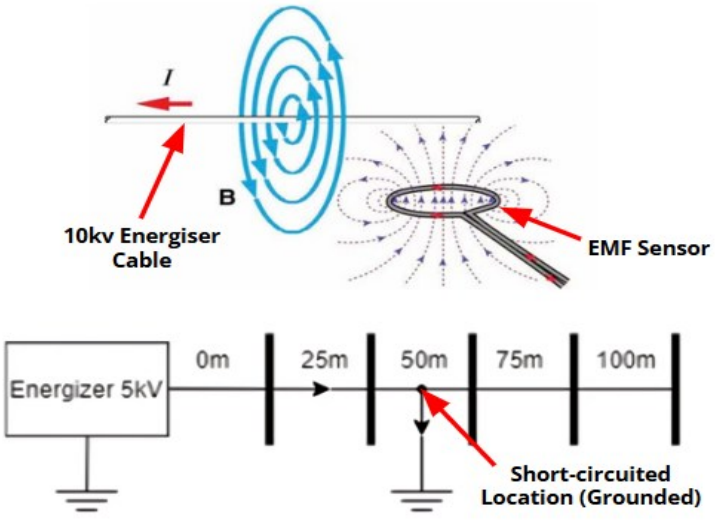

Figure 3. Contactless EMF sensor and conducted test setup [13].

https://doi.org/10.31436/iiumej.v27i1.3720

Although the authors suggested that the coil-based sensor could be mounted on a drone for field deployment, such an implementation would require stable low-altitude flight, precise coil-wire alignment, and mitigation of electromagnetic interference (EMI) from the drone's own electronics and the surrounding environment. These constraints substantially increase the operational complexity and cost, making routine deployment along rural fences impractical.

A study by Ali et al. [14] implemented a system to monitor the health of an electric fence using an Arduino and a GSM module for data transmission. In this work, the current is measured between a power supply (battery) and an electric fence energiser input. The status of the electric fence is determined by the current measured between the battery's positive terminal and the energiser's positive terminal. A microcontroller (Arduino) is used to collect and analyse data before transmitting it to an online server (Blynk) via a 4G GSM module. Figure 4 illustrates the system's process for delivering current sensor data to a mobile phone for monitoring.

In this system, notifications are generated via the Blynk app and are simulated under various power supply fault conditions in an actual fencing environment. However, it fails to address the critical issue of fault localisation triggered by short circuits, and it requires manual inspection and identification. This limitation highlights the need for more comprehensive monitoring solutions that can accurately identify and locate a broader range of fault types.

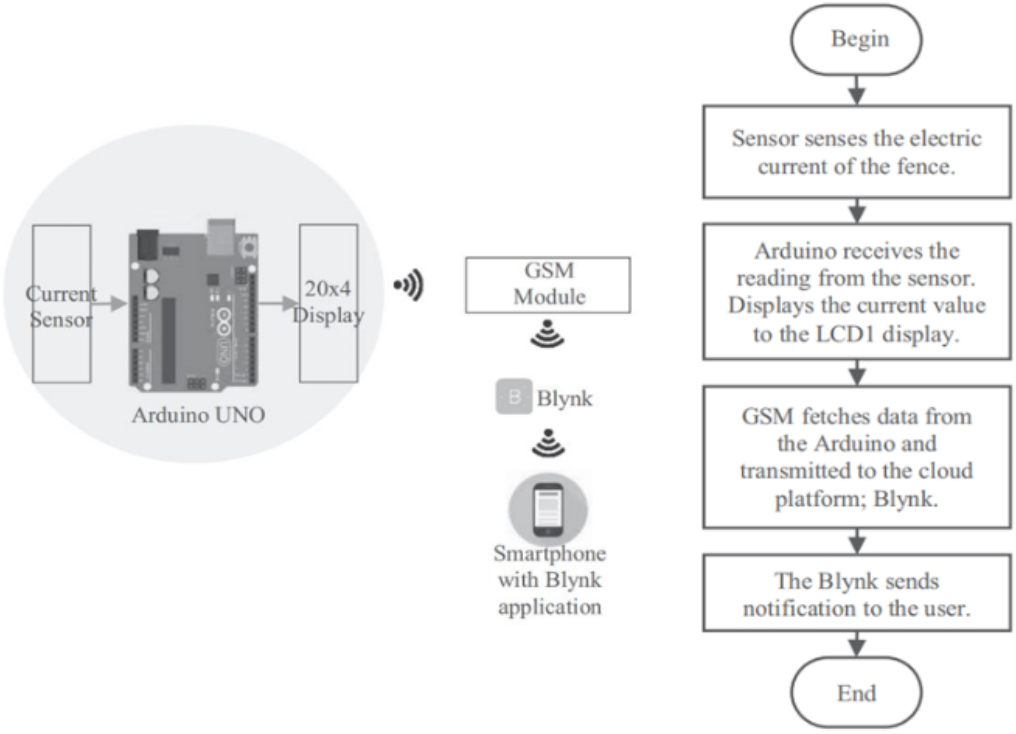

Figure 4. Monitoring system for electric fence architecture and flowchart [14].

Yunus and Zainal [15] proposed an IoT-based intelligent monitoring system for farm electric fences powered by a stand-alone solar energy supply. The architecture employed a microcontroller-based unit (ESP32S) with wireless communication capability (WiFi) to transmit fence parameters to a remote interface. Theoretically, this approach enables farmers to continuously monitor fence performance and receive notifications of abnormal operating conditions without requiring manual inspection.

https://doi.org/10.31436/iiumej.v27i1.3720

In their implementation, the incorporated sensor (as shown in Figure 5) measures key electrical characteristics of the fence circuit, including output voltage, current draw, and battery status [15]. The system was installed in a farm setting and evaluated over two days to assess its stability and effectiveness under real conditions. Measurements of solar input and battery state of charge were also taken to assess the power supply's self-sufficiency. Data collected from the sensors were transmitted to a central dashboard, where operators could observe trends and detect potential anomalies in near-real time.

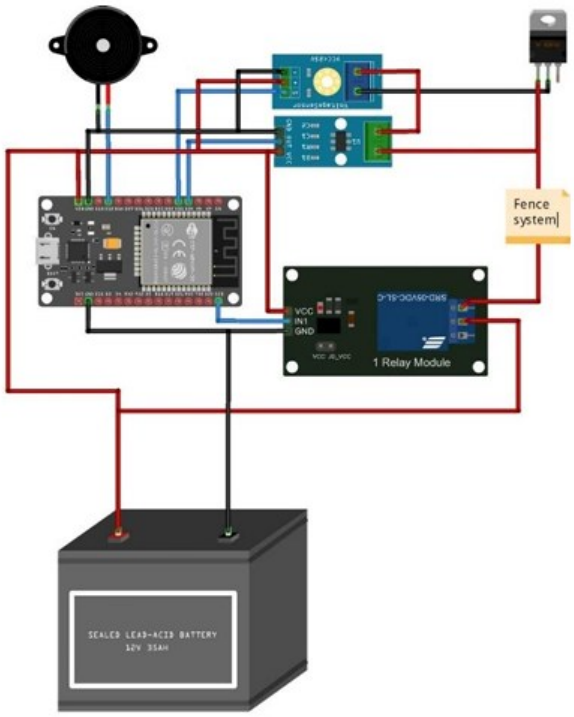

Figure 5. IoT-based Intelligent System Circuit Connection [15].

The results reported by Yunus and Zainal indicated that the system successfully captured and communicated variations in fence voltage, current, and power supply parameters throughout the test period [15]. The prototype demonstrated that IoT-enabled monitoring can enhance situational awareness of electric fence conditions and support proactive maintenance. However, their study did not implement or evaluate a mechanism for pinpointing the location or exact nature of faults along the fence line. This suggests that further research is needed to extend such systems beyond parameter monitoring to include precise fault localisation and classification, to implement a more effective monitoring system for electric fences.

Based on the data summarised in Table 1, four distinct approaches to electric-fence monitoring have been reported by Tennakoon et al. [12], Al-Bahadly and Simpson [13], Ali et al. [14], and Yunus and Zainal [15]. The design proposed by Tennakoon et al. can accurately detect wire breakages but is limited to series-connected, ground-return electric fences and is therefore not directly applicable to SPEG's parallel all-live configuration. The contactless method proposed by Al-Bahadly and Simpson demonstrates that fault location can be determined from induced EMF measurements. However, its reliance on specialised equipment and the challenges associated with drone-based deployment reduce its practical suitability for routine field use. By contrast, the system described by Ali et al. [14] and Yunus and Zainal [15] emphasises remote mobile notification but does not address fault-location detection. However, it informed the development of the early-warning component in the present work.

https://doi.org/10.31436/iiumej.v27i1.3720

Table 1. Summary of existing electric fence monitoring technologies

Reference	Fault Detection	Remote Monitoring	Complexity	Practicality
Tennakoon et al. [12]	Yes.	Yes. Provides remote mobile notifications.	High. High risk of system failure.	Medium. Not applicable to SPEG electric fences.
Al-Bahadly and Simpson [13]	Yes.	No.	High. Specialist Dependent.	Low. Challenges associated with drone-based deployment and coil alignment in the field.
Ali et al. [14]	No. Only the power supply is monitored.	Yes. Provides remote mobile notifications.	Low.	High.
Yunus and Zainal [15]	No. Only power supply analysis.	Yes. Provides remote mobile notifications.	Low.	High.

2.2. Review on IoT integration with Wireless Communications

Electric fences are typically developed in remote forested and rural environments to confine animals within their natural habitats. These areas often lack essential infrastructure, such as electricity and potable water, rendering them generally uninhabitable for humans. Consequently, the lack of readily available power sources in these rural settings necessitates the use of batteries and alternative energy sources, such as solar panels [16]. Furthermore, these remote areas are usually far from human settlements and often lack cellular towers, thus limiting communication networks. Limited mobile infrastructure in rural regions poses challenges to the effective implementation of many modern technologies [17].

Technical personnel responsible for maintaining electric fences in isolated rural and forest areas frequently rely on radios and walkie-talkies for communication due to the absence of cellular and internet connectivity. An effective electric fence monitoring system requires access to a dependable communication network to transmit data and alerts to relevant personnel. Sendra et al. [16] had highlighted in their research on smart systems for rural areas that long-distance wireless technologies are the most viable solution for covering such vast expanses. This is where LoRaWAN becomes relevant. The emergence of Long Range (LoRa) and Long-Range Wide Area Network (LoRaWAN) technologies offers innovative long-range wireless communication methods. These technologies present a modern technical solution for communication in rural areas where traditional mobile network coverage is unavailable [17].

The LoRaWAN protocol utilises LoRa modulation, providing low power consumption for devices and an extensive communication range that can span several kilometers [18]. Figure 6 illustrates a typical LoRaWAN system architecture. A standard LoRaWAN system is structured into three distinct layers: the application layer, the network layer, and the server layer. In the application layer, sensors are connected to end devices, which function as transceivers capable of both receiving and transmitting data. These end devices process data collected by sensors and communicate with a LoRaWAN gateway to transmit the information. Within the LoRaWAN network, these end devices transmit data asynchronously to any gateway within their signal range [18]. This data transfer occurs within the network layer, utilising the LoRaWAN bandwidth.

https://doi.org/10.31436/iiumej.v27i1.3720

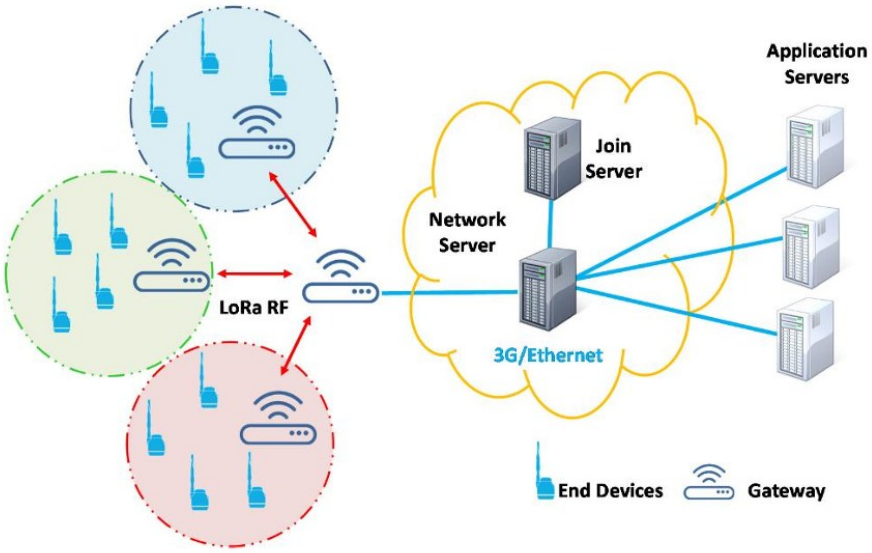

Figure 6. LoRaWAN system architecture [16].

The LoRaWAN gateway is a central component within a LoRaWAN system. In a basic LoRaWAN network design, a single gateway can typically support numerous end devices and manage their data transmissions. However, as shown in Figure 6, end nodes can also send data to gateways in their vicinity, which then relay it to a centralised gateway connected to the internet. Subsequently, the gateway establishes a connection to the server layer via technologies such as 4G LTE or WIFI. This constitutes the server layer.

Within the server layer, the gateway forwards the received data to a LoRaWAN server. Industrial users often prefer the ChirpStack server due to its robustness, enhanced customisation options, and security features. In contrast, the general community frequently utilises The Things Network (TTN), which is known for its user-friendliness and community-driven approach. From these LoRaWAN servers, the collected data can be stored in a local database or in a cloud storage platform (e.g., Google Cloud, Microsoft Power BI, or Amazon Web Services). This type of cloud integration can be achieved by calling APIs via the TTN web page. From this point, users can choose to perform data analysis, apply filters, set up notifications, or create monitoring dashboards for data visualisation. The TTN application servers can be configured to send messages via SMS or email to the maintenance departments of relevant authorities regularly or when specific issues arise [19].

A study by Sendra et al. [16] provides a comparison of LoRa with various other Internet of Things wireless communication protocols, as summarised in Table 2 (and visualised in Figure 7). Specific IoT applications, including the one discussed in this paper, require characteristics such as long-range capability, low data transmission rates, and minimal energy consumption. Short-range technologies such as Zigbee or personal area networks are unsuitable for environments requiring extensive coverage, leading to the exclusion of Zigbee and Wi-Fi standards from this analysis. While NB-IoT meets these requirements, its reliance on existing 3GPP networks and the need for costly network deployment limit its applicability relative to SigFox and LoRa. Technically, SigFox and LoRa share similarities. However, LoRa distinguishes itself by its open protocol and its ability to establish a cost-effective network, unlike SigFox, which relies on operator network coverage [16].

https://doi.org/10.31436/iiumej.v27i1.3720

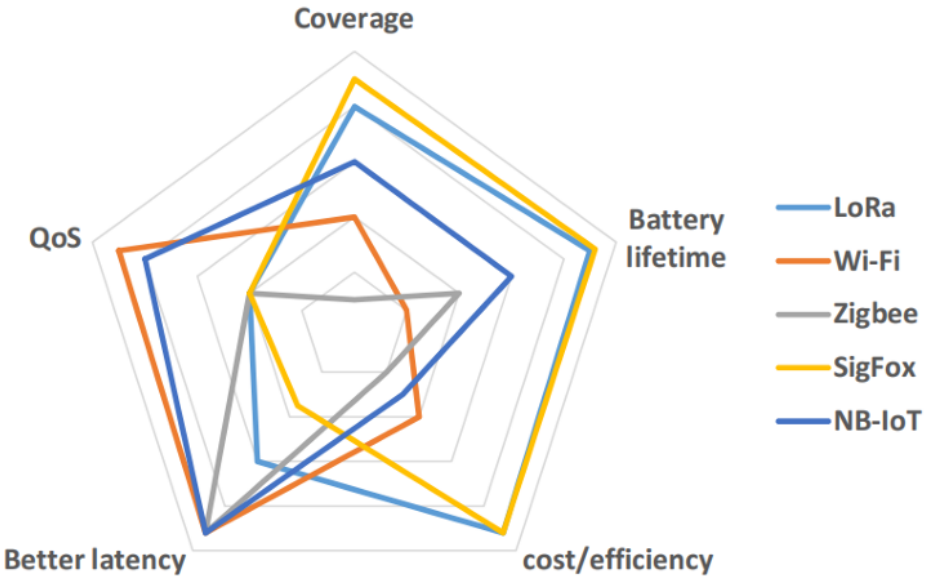

Figure 7. Comparison between IoT technologies [16].

Hence, based on previous studies, a LoRa/LoRaWAN communication network is deemed the most appropriate for the research proposed in this paper. This suitability stems from its broad coverage area, low cost, and low power consumption, which are critical to the successful implementation of this research.

Table 2. IoT communication technologies comparison [16].

	Lora	**Wifi**	**Zigbee**	**SigFox**	**NB-IoT**
Frequency	868 MHz (EU); 915 MHz (USA); 433 MHz (Asia)	2.4 GHz and 5 GHz	868 MHz (EU); 915 MHz (USA); 433 MHz (Asia); 2.4 GHz	868 MHz (EU); 915 MHz (USA); 433 MHz (Asia)	Depends on the frequency licensed to LTE
Standard	IEEE802.15.4g, LoRa Alliance	IEEE802.11	IEEE802.15.4	SigFox (Owner)	3GPP Standard
Coverage	5 km (urban), 20 km (rural)	50 m (indoor), 40 km (outdoor, as a function of the visibility)	10-100 m	10 km (urban), 40 km (rural)	1 km (urban), 10 km (rural)
Modulation	LoRa, FSK, GFSK	BPSK, QPSK, 16 QAM, 64 QAM, 256 QAM, 1024 QAM	BPSK, OQPSK	BPSK, GFSK	QPSK, OFDM (DL, SC-FDMA (UL))
Power Consumption	Low	High	Medium-Low	Low	Low
Theoretical Data Transfer Rate	22 kbps (LoRa), 100 kbps (GFSK)	2.4 Gbps (IEEE802.11 ax, 2 streams with 1024 QAM)	250 kbps at 2.4 GHz, 20 kbps at 868 MHz, 40 kbps at 915 MHz	100 bps	10 Mbps
Price of End Devices	3-5 €	3-5 €	2-5 €	>2 €	>20 €
Price of Gateway	100 € Gateway/ >1000 € Base station	20-600 € Gateway	40-1000 € Gateway	4000 € Base station	15000 € Base station

https://doi.org/10.31436/iiumej.v27i1.3720

3. RESEARCH GAP

Existing remote monitoring technologies for electric fences, such as Tennakoon et al. [12] and Al-Bahadly and Simpson [13], each provide only partial functionality and involve complex, case-specific implementations. Tennakoon et al. [12] designed a system that operates only with a ground-return electric fence and updates fault detections at 15-minute intervals via 4G GSM, thereby delaying the detection of sudden faults and restricting its use in areas without coverage. Similarly, Ali et al. [14] monitor only the power supply of the electric fence via 4G, which neither detects nor localises faults on the fence itself. Al-Bahadly and Simpson [13] measure voltage and current using a coil antenna and propose a drone-operated system. However, the proposed method has not been tested on an actual electric fence architecture.

Electric fences have shown strong potential for mitigating Human-Elephant Conflict (HEC), yet they are prone to voltage drops, short circuits, and structural deformations [12]. To address these issues, a monitoring system capable of integrating multiple measurement parameters is needed. The required parameters include the detection of high-voltage pulses (up to 10 kV), short-circuit fault localisation at 10 m intervals, and the fence leaning angle for structural stability. Data from these sensors also need to be transmitted wirelessly in near-real-time (at 1-minute intervals), a reporting interval consistent with best practices in other safety-critical infrastructure, such as pipeline damage sensing [20].

In-place wireless sensor nodes were selected over wired or drone-based methods due to their suitability for long, remote electric fence lines. Wired systems entail high installation and maintenance demands in large-scale infrastructure, whereas wireless nodes offer greater deployment flexibility and lower costs [21]. Drone-based inspections, while applicable for rapid area surveys, are limited by short flight times, weather, and frequent battery changes, making them unsuitable for continuous or minute-scale monitoring [22].

In this study, a single sensor node is developed that integrates a high-voltage (10 kV) sensor, a voltage-drop sensor for short-circuit localisation, and a gyroscope sensor for structural monitoring. This sensor transmits updates at one-minute intervals rather than the 15-minute cycles used in [12]. Data transmission is carried out via LoRaWAN, a low-power, long-range network that operates in areas with limited cellular coverage. While LoRaWAN requires an upfront investment in gateways, its lower energy consumption and absence of recurring data fees make it more practical than cellular solutions for rural, resource-constrained environments.

The functions of each proposed sensor and its role in the monitoring system are summarised in Table 3. To monitor the electrical health of an electric fence, a sensing mechanism capable of measuring up to 10kV is required. Additionally, to locate a short circuit on an electric fence, a voltage-sensing method is utilised by measuring the voltage drop along the fence. The structural integrity of an electric fence is monitored by measuring its leaning angle. In summary, a 10kV voltage sensor measures electric potential fluctuations. A DC voltage sensor measures voltage drops to locate short circuits. Finally, gyroscope sensors monitor structural deviations, which may indicate potential physical damage.

The integration of these diverse sub-sensors enables a multi-faceted approach to fault diagnostics. By synergistically combining these sensors and integrating them with IoT technologies (via LoRaWAN), technicians can remotely obtain a comprehensive understanding of fault scenarios at each monitoring node along the fence and expedite maintenance.

https://doi.org/10.31436/iiumej.v27i1.3720

Table 3. Sensors proposed for each malfunction.

Fault Type	Sensor Used	Sensor Response	Action Taken
Voltage Drop	10kV Voltmeter	Detects a drop below the threshold.	Alert sent to the technician. Maintenance scheduled.
Short Circuit	DC Voltage Sensor	Detects voltage drops.	Alert sent to the technician. Fault location identified.
Structural Damage	Gyroscope	Detects tilting or leaning of the fence.	Alert sent to the technician. Structural repairs initiated.

4. METHODOLOGY

To achieve comprehensive monitoring of electric fence integrity, an integrated sensor system was developed that incorporated a 10kV voltage sensor, a DC voltage sensor, and a gyroscope sensor. This system addresses critical operational challenges, including structural deformation, voltage fluctuations, and short-circuit faults, which are prevalent in electric fence systems designed to deter large animals such as elephants.

As illustrated in Figure 8, the developed system is divided into two components: the sensor block and the communication network block. The sensor comprises three sub-sensors: a 10 kV sensor, a DC-voltage sensor, and a gyroscope sensor. These sensors transmit raw data to a main Microcontroller Unit (MCU), an STM32. The STM32 processes the raw sensor data and compiles it into a 50-bit message. The MCU is also connected to an RFM95, which equips the sensor with LoRaWAN communication capabilities. The MCU then sends the processed sensor data to a central LoRaWAN gateway, which starts the data acquisition process. The gateway, connected to the internet via 4G LTE, then sends the data to The Things Network (TTN), which triggers a Fetch API request. The Fetch API in TTN pushes data from TTN to a Google server for analysis and storage. The data is stored in Google Sheets and analysed for anomalies exceeding the configured threshold. For any anomalies, a notification will be sent to the personnel involved to rectify the electric fence. The stored data is also processed and presented in a dashboard within a web application.

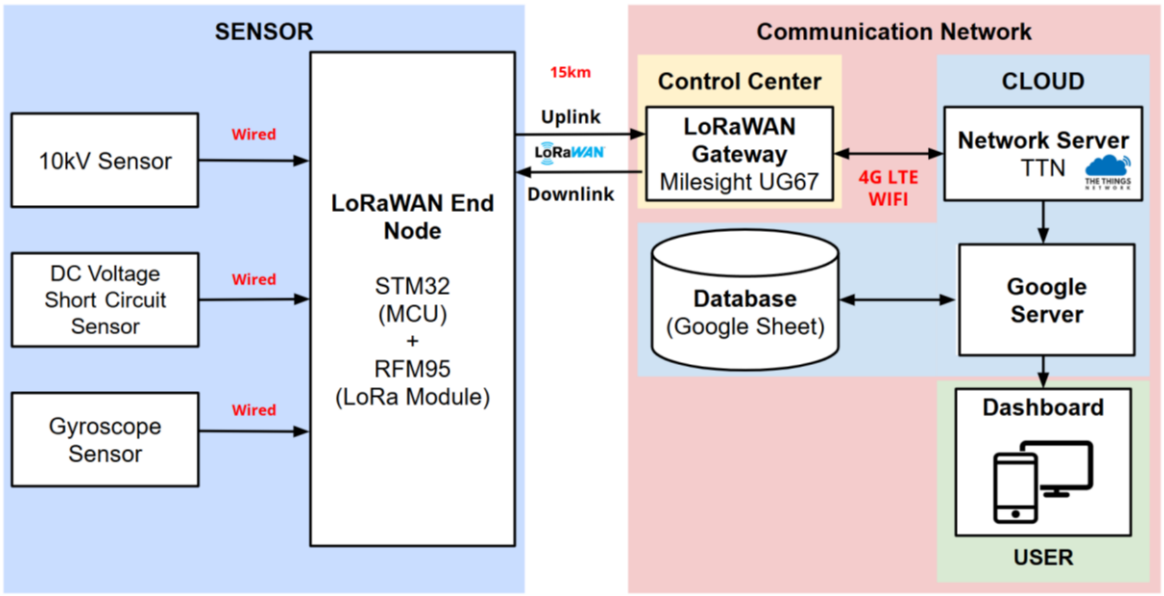

Figure 8. System architecture.

https://doi.org/10.31436/iiumej.v27i1.3720

The system requires a LoRaWAN gateway that is readily configured to the appropriate frequency, operating at 915 MHz in the Australian band (AU915). The monitoring system begins with the measurement of the sensors. Figure 9 illustrates the overall operation of the sensor system, in which the MCU first boots up, followed by the other modules. Once the sensors are powered on, the gyroscope is calibrated to offset all angles to 0°. Subsequently, the sensor data is transmitted to TTN, and the board enters sleep mode. Unless a button is pressed, the sensor will remain in its sleep state until its configured interval is reached. From TTN, the data will be sent to a Google server running Google Apps Script (GAS) for processing and analysis, as previously described. The GAS is also the entity that triggers emails to the appropriate personnel for malfunction detection.

The system's sensor node is divided into two parts: the primary circuit and a voltage divider circuit. As the voltage divider connects directly to a 10 kV energiser supply, its isolation from the main circuit board is paramount to ensure the operational integrity and longevity of the low-voltage components. As depicted in Figure 10, the main circuit, centered around the STM32F103C8T6 Microcontroller Unit (MCU), serves as the central hub for data acquisition, processing, and communication. It is supported by several peripheral modules, including a 915 MHz RFM95 LoRa module for wireless data transmission and an MPU-6050 3-axis gyroscope sensor.

The main circuit is supplied by a 9V battery, regulated by a 3A DC-DC buck converter to provide the necessary voltage levels for the microcontroller and other modules. An FT232 FTDI USB-to-TTL converter is also integrated to facilitate serial communication for programming, debugging, or data logging. The connection labeled 'To Voltage Divider (Load 1-8)' indicates the interface between the main circuit and the isolated high-voltage sensing unit, carrying a scaled-down PWM signal for measurement by the MCU.

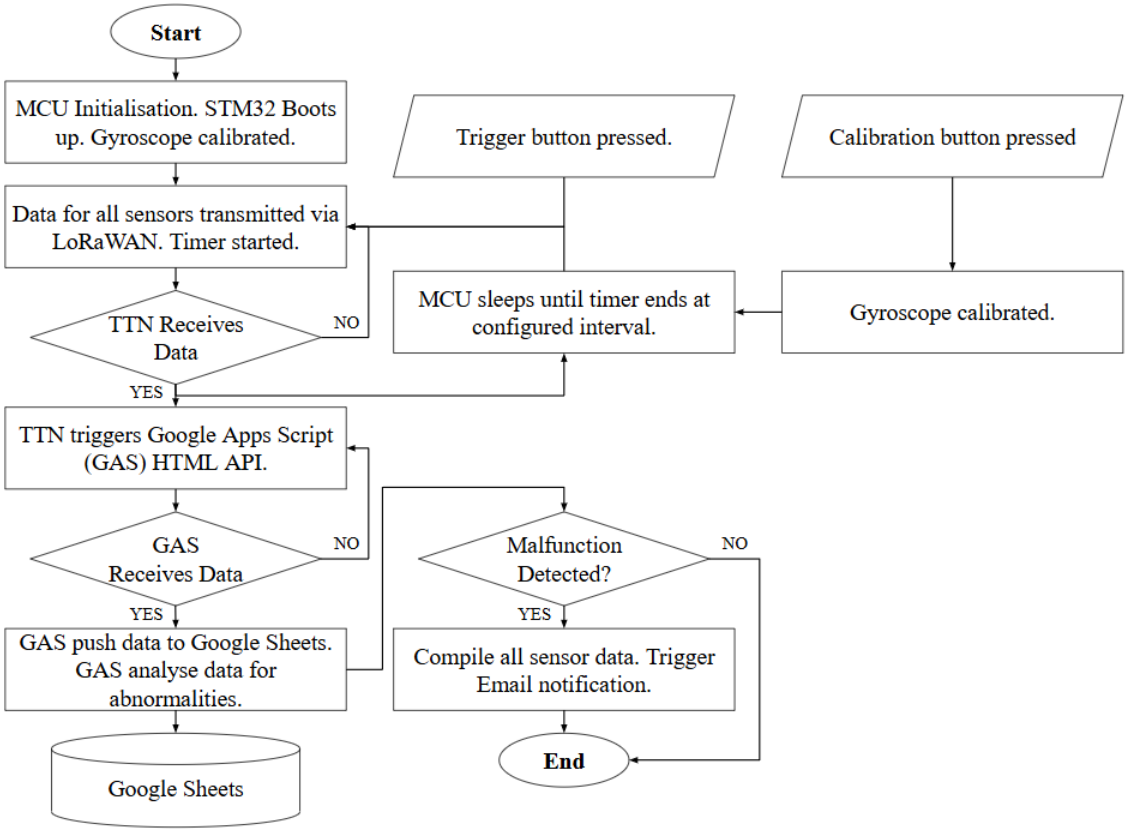

Figure 9. Monitoring system flowchart.

https://doi.org/10.31436/iiumej.v27i1.3720

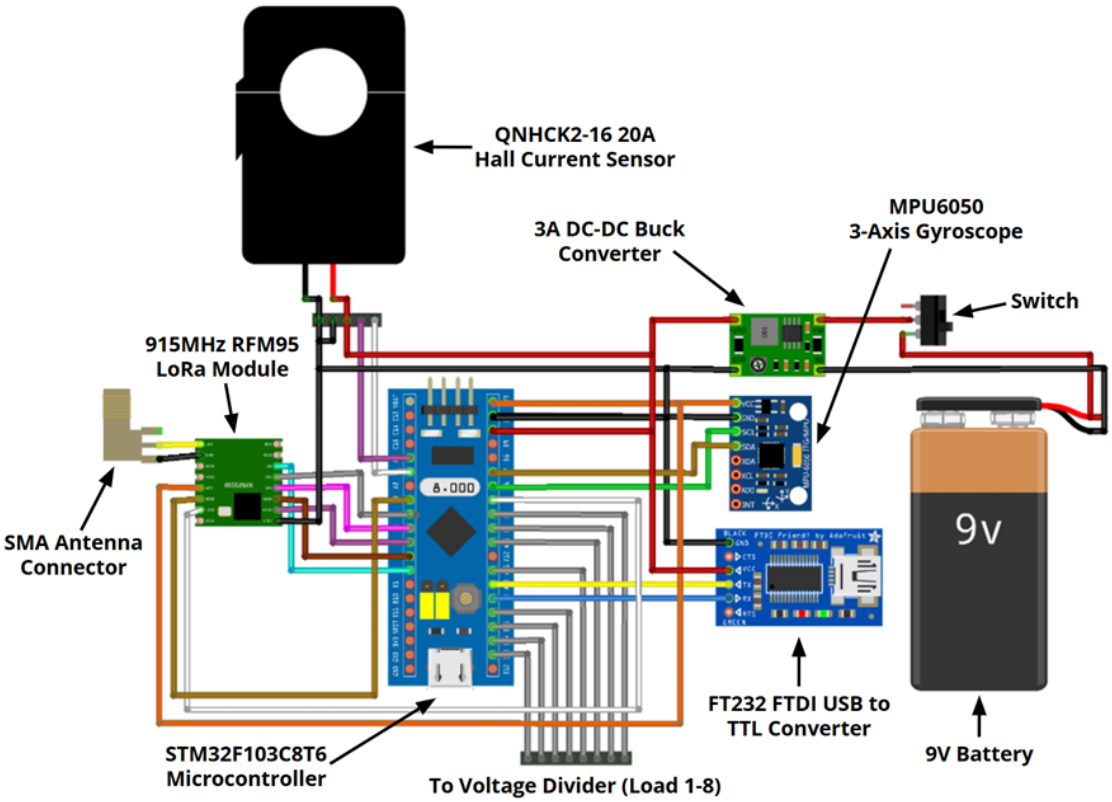

Figure 10. Microcontroller circuit diagram.

A crucial aspect of the sensor node's development and operation involves establishing a communication link with a computer. The STM32F103C8T6 microcontroller, while powerful, lacks a native USB interface for direct communication with a PC's USB port. Therefore, a conversion from the microcontroller's Universal Asynchronous Receiver/Transmitter (UART) serial communication protocol to the PC's USB interface is necessary. This conversion is achieved efficiently by integrating an FTDI FT232 USB-to-TTL converter module, as shown in Figure 11.

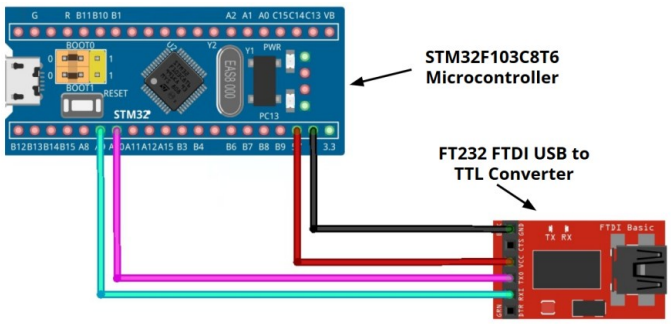

Figure 11. STM32 to FTDI FT232 TTL converter.

The FT232 module acts as a bridge, translating TTL (Transistor-Transistor Logic) level UART signals from the STM32 to the USB protocol understood by the PC and vice versa. It achieves bidirectional communication by connecting the STM32's Tx pin to the FT232's Rx pin and the STM32's Rx pin to the FT232's Tx pin. These cross-connections are essential for bidirectional serial communication. The ground (GND) pins of the STM32 and the FT232 module are also connected to establish a standard reference voltage. By establishing a proper connection between the board and a PC, the sensors may now be configured accordingly.

https://doi.org/10.31436/iiumej.v27i1.3720

4.1. High Voltage Monitoring (Voltage Sensor)

The first sensor developed is a 10kV voltage sensor. This sensor is based on the voltage divider principle, which is commonly used in electric fence voltage testers. A voltage tester was first reverse-engineered and tested to trigger an electronic relay, as shown in Figure 12. The developed high-voltage sensor was tested by dropping the voltage of an electric fence from 10 kV to 8 kV. Preliminary tests, as discussed in the next section, have demonstrated the effectiveness of the detection, and this development was later expanded to measure a broader range of voltage levels in an electric fence.

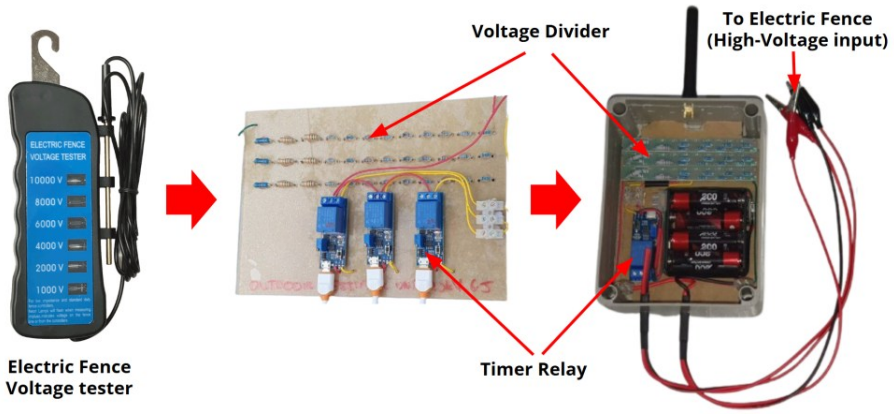

Figure 12. Preliminary 10kv voltage sensor fabricated.

A series of simulation studies has been conducted to determine the appropriate resistance to drop the high voltage to a measurable scale safely. As shown in Figure 13, the simulation involves measuring voltages across 8 resistors, each ranging from 5V to 20V. This voltage will then be connected to a MOSFET circuit to trigger a stable 3.3V to the input PWM pins of the STM32 MCU. In this simulation, all resistance values are calibrated to commercially available specifications. To ensure successful fabrication in the subsequent process, it is also essential to determine appropriate resistor values and power ratings. This is crucial for dissipating heat safely without damaging the resistors, as each resistor will carry a high voltage.

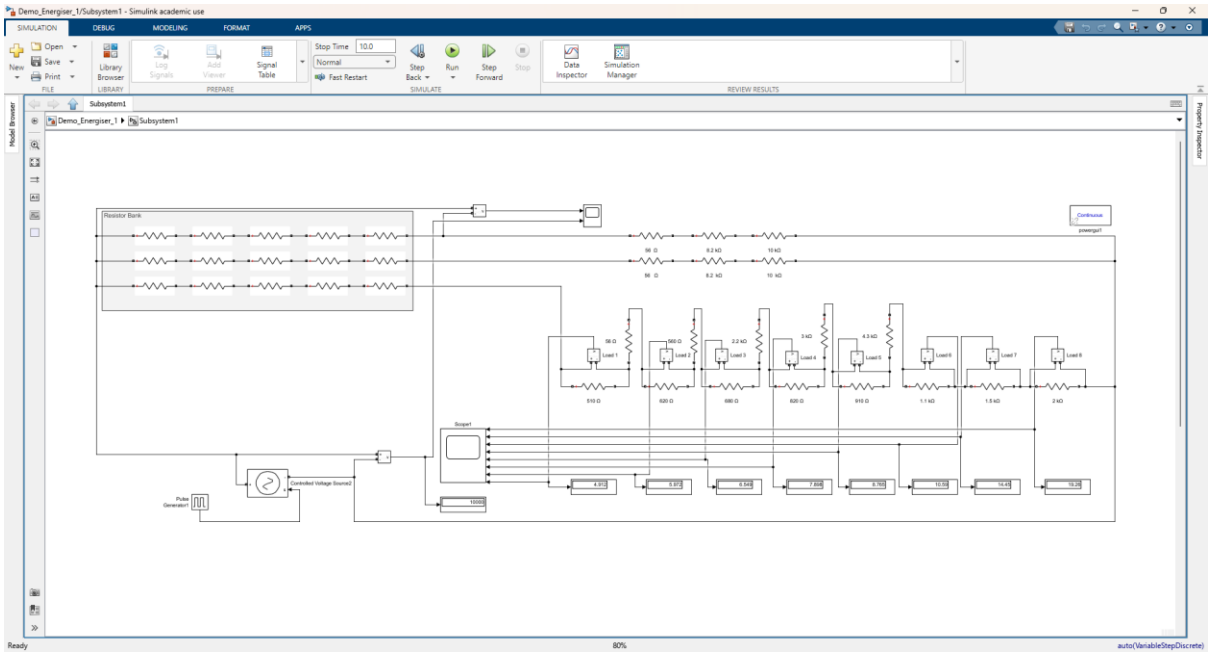

Figure 13. MATLAB-Simulink simulation of 10kV voltage divider.

https://doi.org/10.31436/iiumej.v27i1.3720

4.2. Short-Circuit Localisation (Short-Circuit Sensor)

To locate the short circuit along the electric fence system, a voltage-drop measurement method was proposed. To measure the voltage drop across the electric fence, a stable 12 V DC supply is utilised. As illustrated in Figure 14, this was achieved by connecting the positive terminal of the supply to the electric fence cable and the negative terminal to the ground (the electric fence pole). It is crucial during this process that the electric fence's high-voltage energiser switch be turned off to prevent damage to the 12 V DC supply.

During prototype testing, a manual mechanical switch with a wide contact gap was employed to isolate the 12 V DC supply from the 10 kV energiser for safety reasons. Therefore, the prototype did not operate in real-time during this testing phase. In a deployed system, this isolation will be achieved automatically using a motor-actuated or solenoid-actuated mechanical switch controlled by an MCU, enabling continuous or real-time monitoring without manual intervention. Incorporating such an actuator has been identified as part of future iterations of the system.

This was initially performed automatically using an electronic relay but was later discontinued as the relay contacts were too narrow, resulting in arcing and electrical discharge across the gap. It was found that a relay with a small gap cannot effectively switch off high-voltage pulses exceeding 1 kV. Hence, during testing, the manual switch was utilised, and a motor-actuated version is proposed for full automation during future deployment.

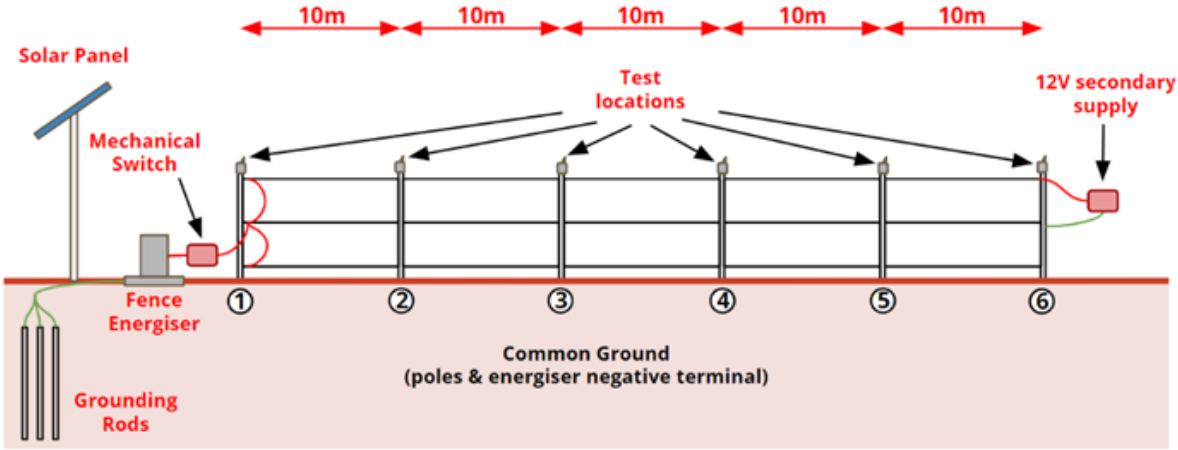

Figure 14. Electric fence voltage drop test setup.

The sensor unit, configured with a voltage sensor, was connected to each pole at the negative terminal and to the fence cable at its positive terminal. Then the electric fence's cable was short-circuited to each pole (connecting it to ground). Subsequently, the sensor measures and records the voltage across each pole.

Based on the test results discussed in the previous section, the proposed voltage-drop measurement approach (using a 12V DC supply and voltage sensors) demonstrated good performance. The method, however, is more suited for shorter electric fence segments, where the distance between monitoring points is limited. For longer electric fence setups, where the voltage-drop approach may increase overall monitoring costs (due to sensor installations), an alternative technique is being explored for future implementation. This method measures the current induced along the electric fence cables using a split-core Hall-effect current sensor (QNHCK2-16, 20 A). Integrated with the MCU for acquisition and processing (as shown in Figure 10), this sensor detects the small EMF-induced current that flows during normal operation and the significantly higher current associated with a short circuit. By placing these

https://doi.org/10.31436/iiumej.v27i1.3720

sensors at successive poles (similar to the previous method, without the 12V supply), it is expected that the point of highest current can be used to infer the short-circuit location.

This proposed approach builds on the fault-finding principle demonstrated in McGillan's handheld electric-fence current sensor [23]. It extends the concept of Al-Bahadly and Simpson [13] toward an automated, in-place monitoring framework, offering a practical direction for future work on long-range electric-fence monitoring.

4.3. Structural Integrity Monitoring (Gyroscope Sensor)

An MPU6050 Inertial Measurement Unit (IMU), featuring a 3-axis gyroscope, was integrated to monitor the electric fence's angular orientation, crucial for detecting potentially hazardous inclinations caused by external factors. The MPU6050 communicates with the STM32F103C8T6 via the I²C protocol, utilising the SDA and SCL lines for data exchange, along with power and ground connections, as shown in Figure 15. The gyroscope measures angular velocity about the X, Y, and Z axes (roll, pitch, and yaw), enabling the system to track the fence's real-time orientation and detect deviations from vertical alignment. The MPU6050 also includes a 3-axis accelerometer, enabling static orientation estimation and improved accuracy through sensor fusion with gyroscope data.

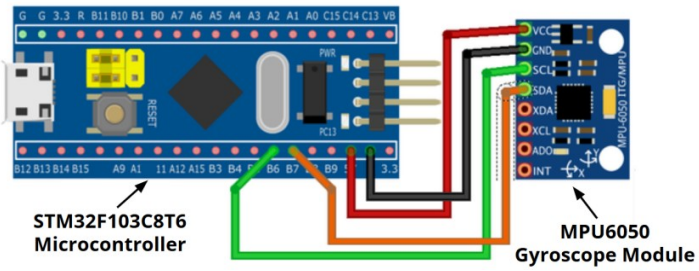

Figure 15. STM32 to MPU6050 connection.

This allows for continuous assessment of the fence's structural condition and the generation of alerts should critical inclination thresholds be exceeded, thereby mitigating the risk of short circuits and ensuring operational safety.

4.4. Data Acquisition and Rural Communication Network

To facilitate data transfer and communication between sensors and the system's IoT infrastructure, the Long-Range Wide Area Network (LoRaWAN) was configured. As illustrated in Figure 16, the system employs a multi-stage communication network to relay sensor data to end users. Sensor nodes utilise LoRaWAN for low-power, long-range wireless transmission to a central gateway. The gateway then uses TCP/IP over its internet connection to forward this data to the TTN Server. Subsequently, the TTN Server communicates with a Google Apps Script running on a Google server via the Fetch API to process and store data. Finally, end users can access the analysed data via a web application interface.

To apply in practice, a conceptual field deployment depicted in Figure 17 illustrates the strategic placement of sensor nodes along the electric fence line, with each node approximately 10 meters apart. These sensor nodes, equipped with an STM32 microcontroller, all sensors, and an RFM95 LoRa module, wirelessly transmit their collected data using the LoRaWAN protocol to a centrally located LoRaWAN gateway. The long-range capability of LoRaWAN is crucial for covering these distances in rural settings, thereby eliminating the need for extensive wired infrastructure. The conceptual field deployment also employs the automated fence actuator previously proposed as a future enhancement.

https://doi.org/10.31436/iiumej.v27i1.3720

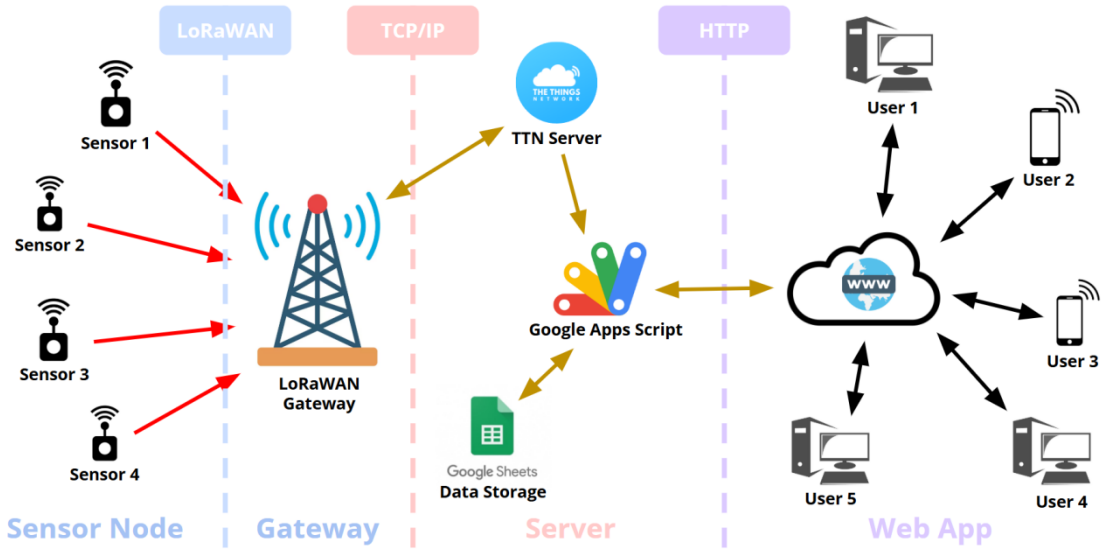

Figure 16. Overall system network topology.

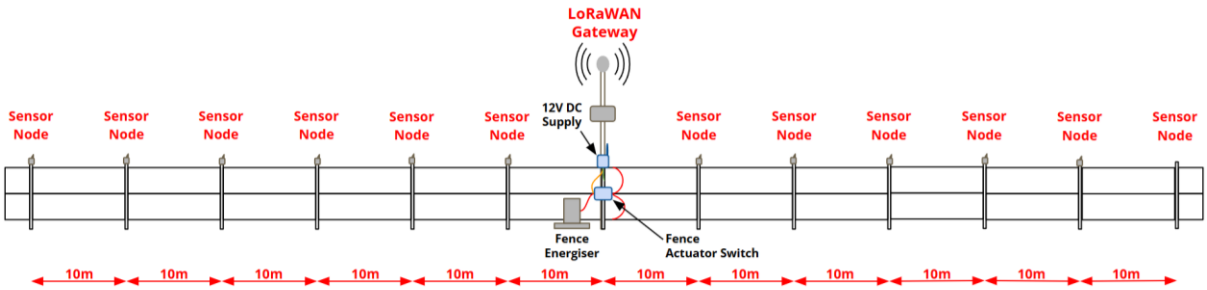

Figure 17. Conceptual field deployment.

The implementation process began with configuring a LoRaWAN gateway. The Milesight UG67 outdoor LoRaWAN gateway is used for this purpose. The gateway connects to the internet via a 4G SIM card. The gateway must be configured according to the region and frequency at which it is used. In this study in Malaysia, the licensed regional frequency is AU915, operating at 915 MHz. This needs to be done in the gateway's web UI. The exact configuration will then need to be applied to The Things Network (TTN) during gateway registration.

An end-node circuit, initially comprising an Arduino microcontroller and an RFM95 module was developed and configured to connect to the TTN server. Subsequently, the RFM95-configured Arduino end node was planned for integration with the MPU6050 gyroscope sensor. However, due to the ATmega328's limited 32 Kbytes of flash memory, integrating the RFM95 and MPU6050 modules consumed more than 80% of the available flash memory, causing errors during board initialization. The microcontroller was changed to an STM32F103C8T6 board with double the flash memory (64 Kbytes). Figure 18 shows the circuit that allows connection between the STM32 and RFM95 boards for LoRaWAN adaptation.

The Integrated Development Environment (IDE) used for this configuration remains the Arduino IDE, as it is compatible with STM32 boards and supports additional configurations and the installation of STM32 libraries. Currently, there are limited libraries that support the AU915 band. However, to apply this region and frequency, the MCCI_LoRaWAN_LMIC

https://doi.org/10.31436/iiumej.v27i1.3720

library must be modified to extend the US915 band to support AU915 via Activation by Personalisation (ABP). Before configuring the STM32, a TTN application and end-device registration must be completed. Because the RFM95 modules are not yet configured with an Extended Unique Identifier (EUI), a Device EUI must be generated and assigned to the STM32 board, along with the Network and App Session Keys generated during TTN configuration. This allows TTN to identify the sensor node when the gateway detects its uplink signal. Upon successful data acquisition, the other sensors were later integrated with the STM32, as shown in Figure 10.

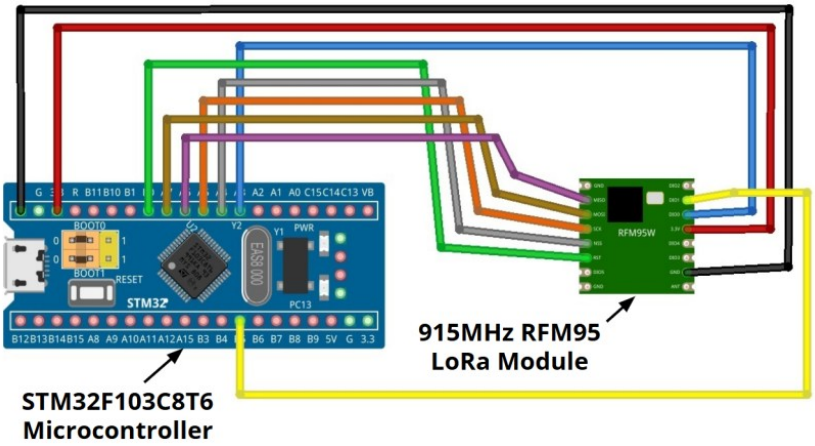

Figure 18. STM32 to RFM95 connection.

A cloud database (Google Sheets) was established to store historical data, enabling data analysis and visualisation via a web-based monitoring dashboard. The dashboard provides real-time indicators of electric fence malfunctions (voltage drop, structural leaning, and short circuit). The web application, accessible via a browser, serves as a manual watchdog for electric fence maintenance, demonstrating the potential of infrastructure monitoring in rural areas. Figure 19 shows the dashboard user interface (UI) operating in a web browser.

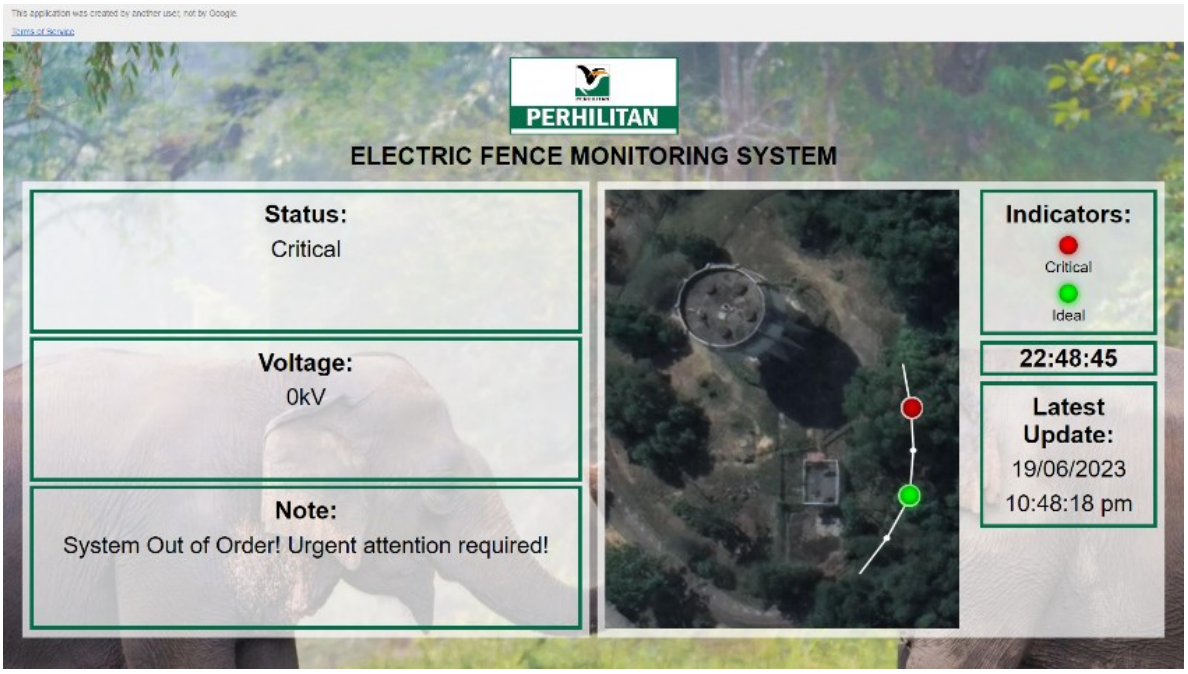

Figure 19. Developed system user interface.

https://doi.org/10.31436/iiumej.v27i1.3720

In addition to the manual watchdog, an automated notification system was implemented to alert technicians of malfunctions. Email notifications were configured to trigger alerts when sensor readings exceed predefined thresholds, indicating system anomalies. This approach, commonly used in industrial monitoring systems, ensures timely notification of site-related issues. Figure 20 shows an example of an email notification triggered. This system enables rapid response to faults, minimising overall downtime.

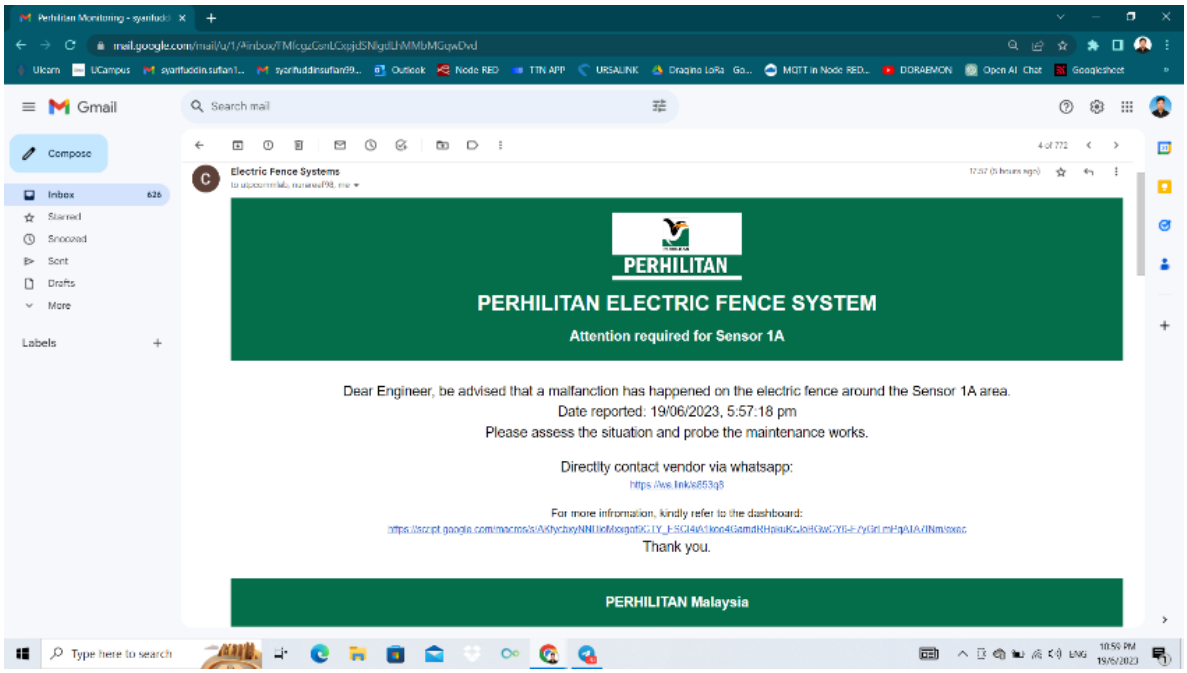

Figure 20. Email notification for fault detection.

4.5. Overall Pin Connection

After all configurations were done with the prototype sensor node, a complete pin configuration was finalised. Figure 21 illustrates the overall pin configurations of the sensor node's core components and MCU. The STM32F103C8T6 interfaces with the MPU6050 via I²C (SDA, SCL), the FT232 for USB communication (Rx, Tx), the voltage divider via digital input pins, and the RFM95 LoRa module via SPI and control pins. For the 915MHz LoRa communication, the RFM95's antenna output (ANT) connects to an SMA connector. To optimise signal integrity and reduce cable and connector losses, the PCB trace between the RFM95's ANT pin and the SMA connector should be kept as short as possible. Additionally, the RF signal paths should be carefully routed away from noise sources on the board. This is crucial for minimising electromagnetic interference and signal loss, thereby improving the Signal-to-Noise Ratio (SNR).

The core components of the final fabricated sensor node are shown in Figure 22. A 3-dBi omnidirectional monopole antenna is used for transmitting and receiving signals and is connected to an SMA connector via a coaxial cable. The placement of all components was also optimized to reduce the risk of short circuits. The fabricated sensor node also includes a Hall current sensor, which was previously proposed for future work.

https://doi.org/10.31436/iiumej.v27i1.3720

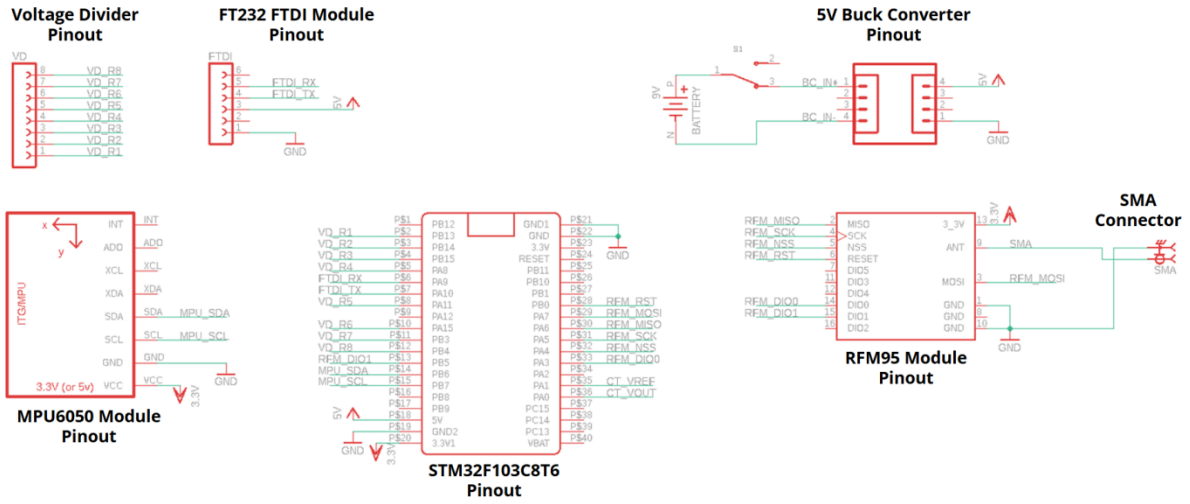

Figure 21. Overall pin connection.

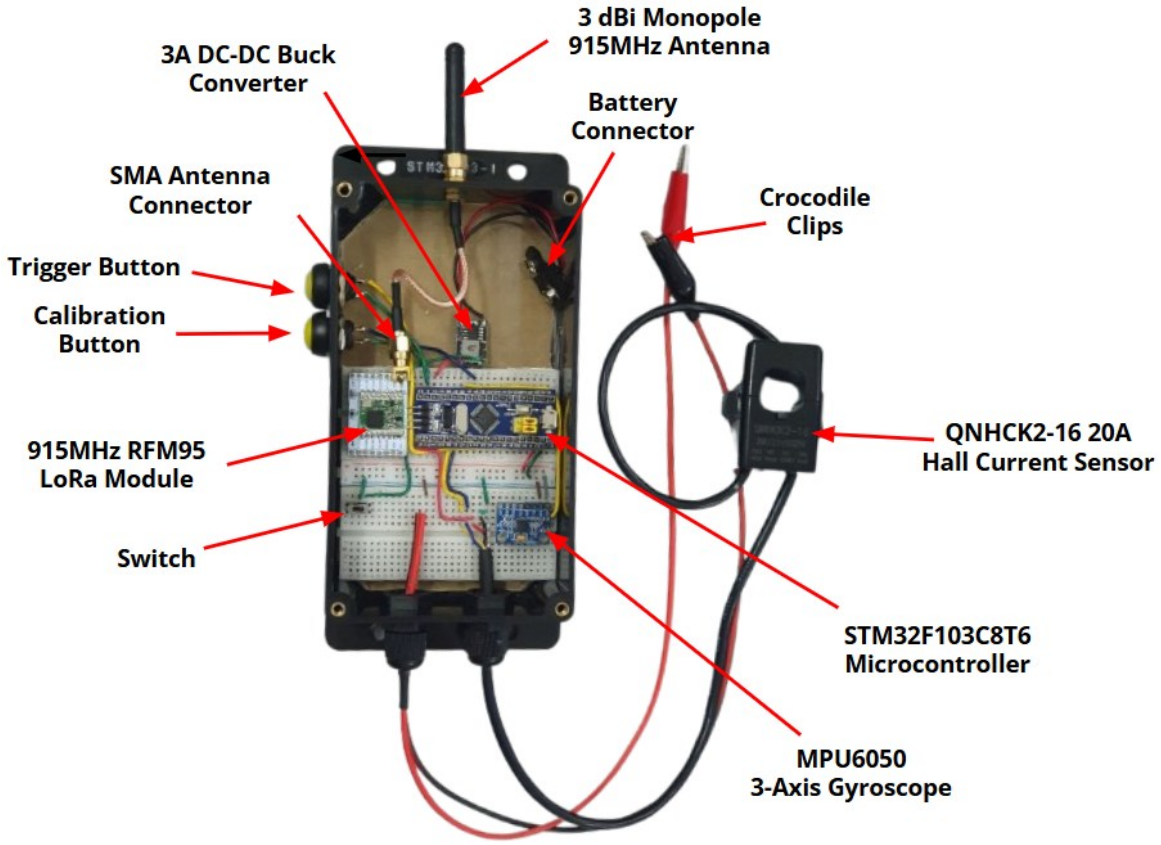

Figure 22. STM32 integrated sensor node.

5. RESULTS AND DISCUSSION

This section presents experimental and simulation results for the designed sensors, as well as the data acquisition and monitoring system configured over the LoRaWAN communication network. The experiments were conducted on a 50-meter electric fence sample provided by the Department of Wildlife and National Parks, Peninsular Malaysia (PERHILITAN). The setup featured 2.5 mm-thick galvanised angle-steel poles, spaced 10 meters apart, and grounded to the energiser's neutral. The fence utilised 2.5mm-diameter galvanised steel cables, energised

https://doi.org/10.31436/iiumej.v27i1.3720

by a 10kV, 6A energiser powered by a 12V SLA battery and a 100W solar panel. All specifications are designed similar to the Sistem Pagar Elektrik Gajah (SPEG) used by PERHILITAN. The test setup is illustrated in Figure 14. The tests were performed outdoors at the UTP campus in Seri Iskandar, Perak, under typical cloudy-day conditions, with an ambient temperature of approximately 33°C and a relative humidity of approximately 59%.

Due to the high electric fence voltage of 10kV, direct oscilloscope capture of the waveform requires safe attenuation through specialised isolation. Hence, this study does not analyse the waveform using an oscilloscope. Instead, the pulse characteristics of the energiser were analysed using the manufacturer's specifications [24], alongside the pulse parameters reported in a previous study by McGillan [23]. Based on [23], common electric-fence energisers generate very short 50-500µs high-voltage pulses between 4kV and 12kV, at a frequency of approximately 0.6Hz. This is consistent with the specifications of the energiser used in the test, which outputs high-voltage pulses of 10kV with a pulse duration of approximately 300 µs at 1.5s intervals (0.67 Hz) [24].

5.1. Voltage Sensor Performance

During this preliminary validation, several tests were carried out on the developed voltage divider circuit. The circuit was made to trigger relays connected in parallel to each resistor, as shown in Figure 12. The circuit was tested on two energiser setups: a 10kV 2.2A energiser and a 10kV 6A energiser. The energiser voltage was reduced by connecting the test circuit's input after a series of resistors (which absorb part of the 10kV supply load).

During testing of the 10kV, 6A energiser, the initial voltage-divider configuration exhibited cracking and visible arc-over of the 20 kΩ, ½ W resistor carrying the highest instantaneous load. This behaviour is consistent with the resistor's power tolerance being exceeded under high-energy pulses, resulting in mechanical failure of the resistive element and subsequent high-voltage discharge across the small physical gap ("arc-over") on the resistor. To address this, the divider network was redesigned into three identical parallel branches with equal total resistance, thereby distributing the pulse current and instantaneous power dissipation across multiple resistors and increasing the effective creepage distance between high-voltage nodes. This modification eliminated the observed arc-over and enabled stable operation under the 6 A energiser conditions. Table 4 shows the test results of the fabricated sensors.

Based on Table 4, the initial circuit determined whether the voltage was 10kV or 9kV (indicated by "YES" in the table), whereas 8kV was not detected (indicated by "NO" in the table). The modified circuit was later tested using the same test scheme as before. The results show that it can detect and determine the voltage of the electric fence (i.e., 10kV or 9kV). The sensor achieved 100% consistency across 10 tests, demonstrating its potential for detecting high DC voltages. This indicates that lower voltages can be detected by expanding the voltage divider circuit.

Table 4. Voltage sensor detection results

Detection	Initial Circuit			Modified Circuit		
	10kV	9kV	8kV	10kV	9kV	8kV
10kV 2.2A Setup	YES	YES	NO	YES	YES	NO
10kV 6A Setup	NO	NO	NO	YES	YES	NO

To detect the lower voltages (2kV to 8kV), the sensor was redesigned using the same concept of a potential divider. The circuit was simulated at these voltages using

https://doi.org/10.31436/iiumej.v27i1.3720

MATLAB/Simulink (as shown in Figure 13). The voltage across all 8 resistors was measured as the voltage was reduced from 10kV to 2kV in 1kV steps. With a 10kV supply, all 9 loads show voltages above 5V. When the supply voltages were reduced by 1kV, the voltage across the loads fell below 5V (see Figure 23).

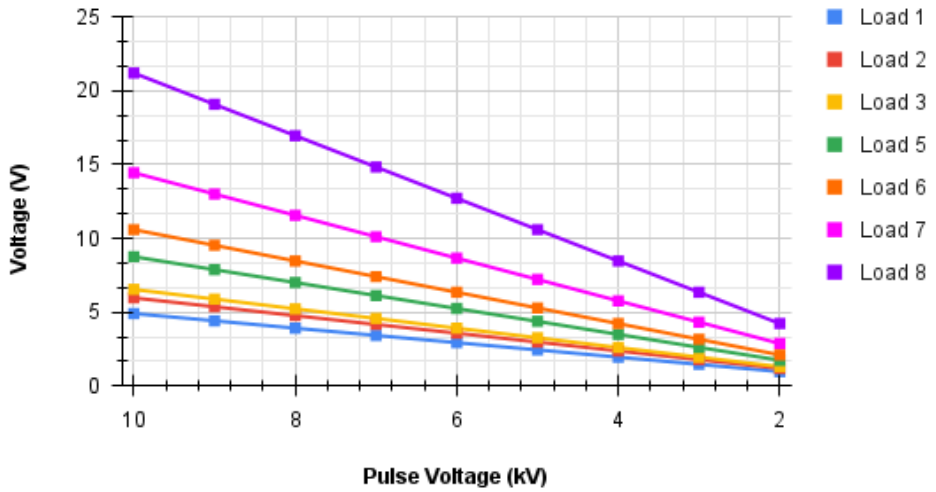

Figure 23. Voltage across each load at different pulse voltages.

The 5V voltage across each resistor will be used to trigger an IRFZ44N MOSFET that controls a 3.3V DC supply. For voltages above 5V, 3.3V will be used as a high digital input to the PWM I/O pins of the STM32 MCU. From the simulation results, reducing the energiser voltage from 10kV to 2kV reduces the total number of high digital inputs to the MCU, as shown in Figure 24. Based on experimental and simulation studies, the designed circuit can accurately determine the voltage level of the electric fence from 2kV to 10kV with a precision of 1kV.

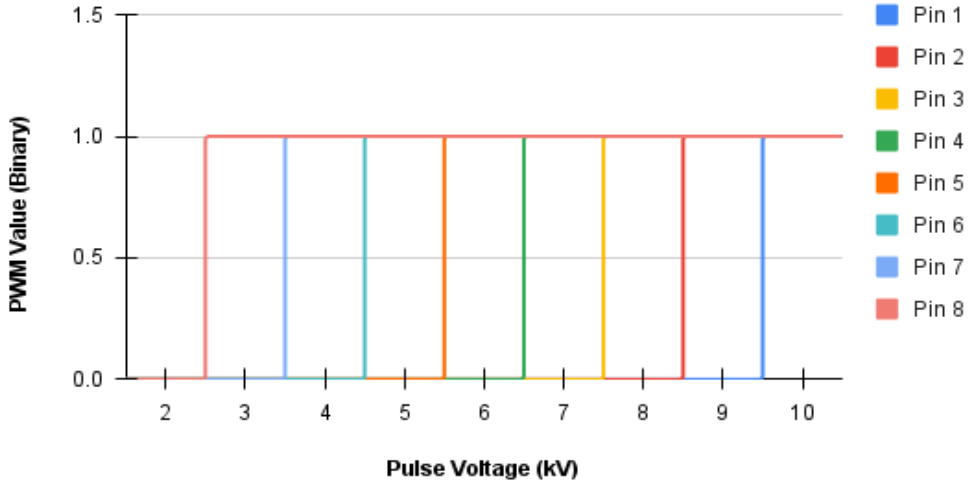

Figure 24. PWM levels from each load connecting to the MCU pins.

5.2. Short-Circuit Locator Performance

The initial short-circuit locator sensor, utilising grounding principles, was tested on the outdoor fence setup as shown in Figure 14. The developed sensor measures the voltage between the fence cable and the pole (ground). Based on the results tabulated in Table 5, under optimal conditions (without a short circuit), the measured voltage is 12V. When the second pole was shorted, the sensor measurement dropped to 0V at the second pole. For each pole, when shorted, the voltage between the cable and the ground falls to 0V. These results are consistent

across all short-circuit locations (poles 2-5) and were cross-checked using a conventional multimeter. This shows that, with a voltage sensor and a secondary 12V DC supply, the location of the short circuit can be deduced.

Table 5. Short-circuit locator sensor using a voltage-drop test.

Pole	Sensory Element	Voltage at optimum (V)	Short-Circuited Pole			
			Pole 2	Pole 3	Pole 4	Pole 5
1	Multimeter	12.09	11.92	12.03	12.03	12.04
	Sensor	11.99	11.92	11.92	11.92	11.94
2	Multimeter	11.74	0.00	7.27	6.27	7.78
	Sensor	11.20	0.00	7.07	6.09	7.54
3	Multimeter	11.38	4.09	0.00	5.75	7.42
	Sensor	11.25	4.19	0.00	5.53	7.14
4	Multimeter	11.30	4.45	6.96	0.00	7.22
	Sensor	11.23	4.29	6.77	0.00	7.05
5	Multimeter	11.36	4.39	6.98	5.68	0.00
	Sensor	11.00	4.22	6.67	5.46	0.00

While the 12V DC voltage-drop approach demonstrated consistent performance at 10m intervals, extending this configuration to multi-kilometre fence segments would proportionally increase the number of required sensor nodes, with associated cost and maintenance considerations for installations such as PERHILITAN's multi-kilometre SPEG systems. According to SPEG guidelines, a single energiser bay can extend to approximately 4km [6], which would necessitate around 400 sensor units for complete short-circuit coverage at 10m spacing. With an estimated cost of RM 500 per sensor unit, the total expenditure for monitoring one bay could reach RM 200,000, highlighting the importance of scalable solutions for long-range deployments.

As outlined in Section 5, a Hall-effect current-sensing technique employing split-core sensors such as the QNHCK2-16 has been identified as a potential alternative for long-range fault localisation. Although this method has not yet been experimentally validated within the present study, its feasibility is supported by the principles demonstrated in [13] and [23]. Accordingly, its implementation and performance evaluation are planned for future work.

5.3. Gyroscope Sensor Performance

The circuit shown in Figure 15 was fabricated and tested to evaluate the gyroscope sensor's reliability in detecting the leaning of the electric fence setup. The experiment involved inclining a pole in the X and Y directions at specific angles, which were measured using a digital angle meter attached to both a reference pole (vertical) and the test pole (leaning), as shown in Figure 25. Initial calibration established all axes at 0° when the pole was vertical. Measurements were then recorded from 0° to 45° in 5° increments, with ten readings taken at each angle for both axes.

https://doi.org/10.31436/iiumej.v27i1.3720

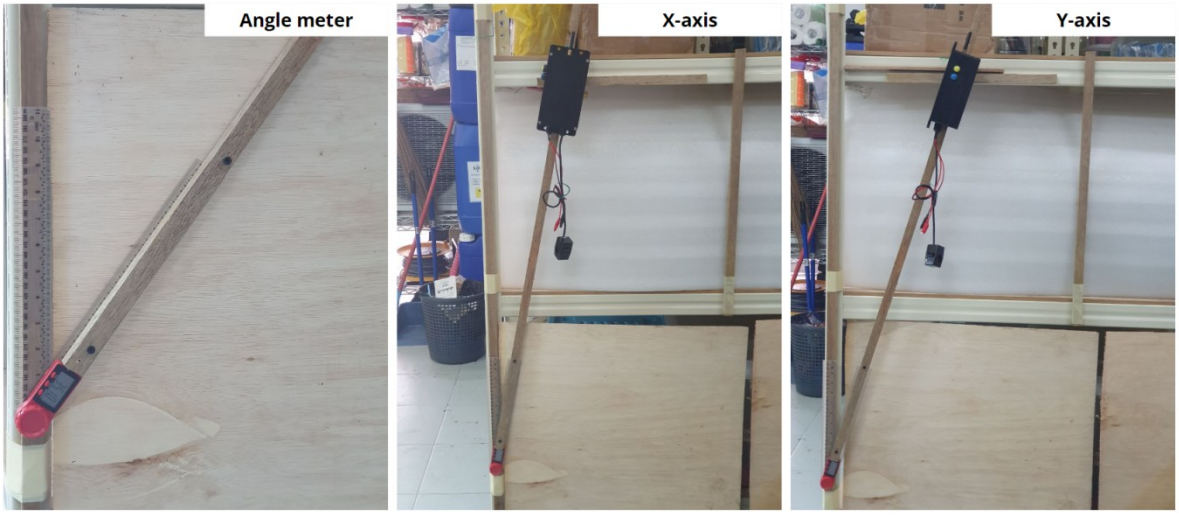

Figure 25. Indoor gyroscope test setup.

During initial testing, the MPU6050 sensor, when mounted directly on the circuit board, produced inaccurate X- and Y-axis readings. This included a high degree of variability along the X-axis and a nonlinear relationship between the actual and measured Y-axis angles. A diagnostic review identified three primary sources of error:

- *Axis misalignment*: the sensor had been oriented with its Y-axis vertical to the ground. According to the MPU6050 datasheet [25], the 'Orientation of Axes of Sensitivity and Polarity of Rotation' indicates that, for correct use in this configuration, the Z-axis should be perpendicular to the ground, which differs from the alignment used in the initial tests.
- *Mechanical instability*: the outdoor test poles were insufficiently constrained and gradually shifted under cable tension and gravity, causing inconsistent axis references across test repetitions.
- *Input disturbance*: angle readings were manually triggered by pressing a button on the sensor, introducing transient motion that distorted measurements.

Corrective measures were implemented before repeating the tests. The sensor was reoriented so that its Y-axis pointed upward, thereby making the MPU6050 board perpendicular to the sensor node board. Test poles were clamped to rigid brackets to maintain consistent orientation, and data acquisition was automated at one-minute intervals to eliminate button-press artifacts.

Following these adjustments, the repeated tests yielded stable, linear results. Scatter plots for both axes are shown in Figure 26 and Figure 27. Based on linear regression analysis of the two test datasets, the MPU6050 gyroscope sensor exhibited high linearity and accuracy for X- and Y-axis measurements under the tested conditions. The maximum deviation between measured and actual angles for the X-axis occurred at 40° (1.20°), and for the Y-axis at 45° (2.02°). Linear regression analysis comparing the sensor's output to actual angles measured by a digital protractor across a range of 0° to 45° yielded coefficients of determination (R^2) of 0.9991 for the X-axis and 0.9990 for the Y-axis. These values indicate a strong positive linear correlation across both axes, corresponding to an accuracy of approximately 99.9%.

https://doi.org/10.31436/iiumej.v27i1.3720

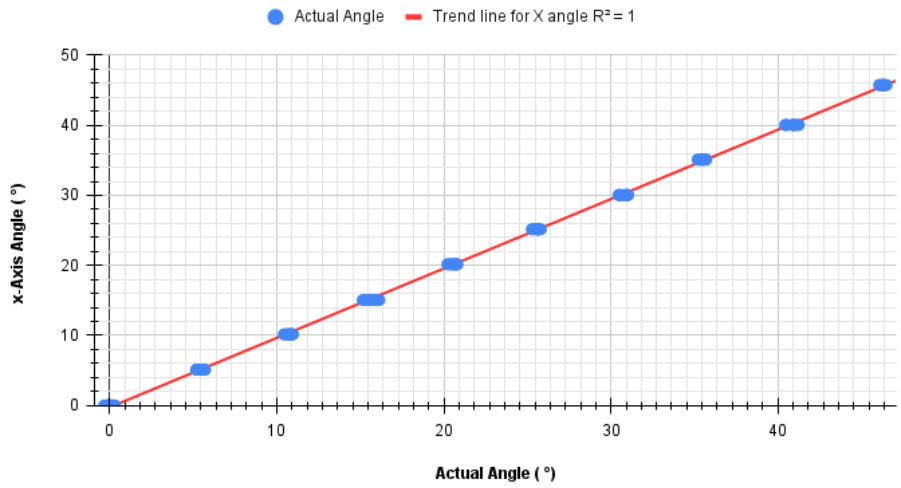

Figure 26. Scatter plot for gyroscope X-axis.

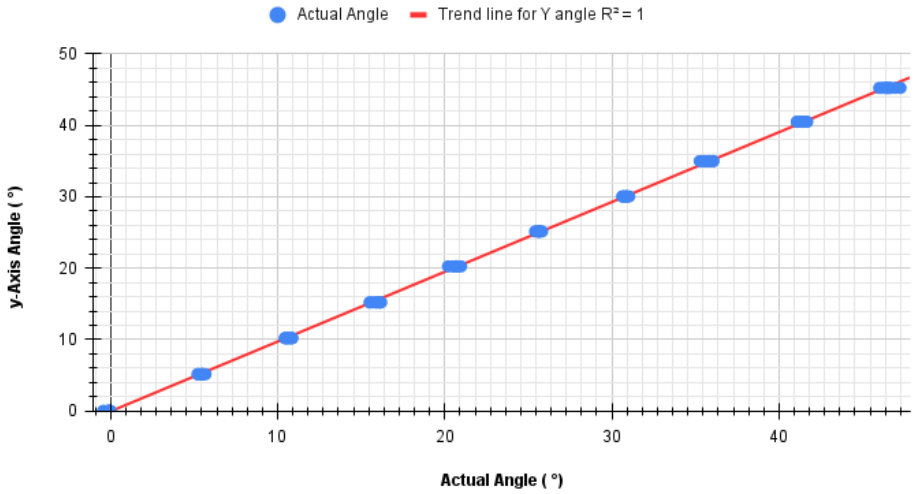

Figure 27. Scatter plot for gyroscope Y-axis.

5.4. Data Acquisition System Performance

The developed sensors were integrated into a LoRaWAN network via a Milesight UG67 industrial outdoor gateway and RFM95-equipped STM32 end nodes. Data were stored in a cloud-based spreadsheet (Google Sheets) and visualised on a web-based dashboard, which also generated automated notifications, as shown in Figures 19 and 20. The system operated continuously for 30 days without data loss, demonstrating its suitability for remote infrastructure monitoring.

To quantify the communication performance, an internal range test was conducted within the UTP campus compound. The UG67 gateway was installed on a 4 m pole at an altitude of 84 m, and the sensor node was moved in 100 m increments up to 1.3 km (13 test points). Figure 28 shows the test layout.

https://doi.org/10.31436/iiumej.v27i1.3720

Figure 28. Range testing conducted in the UTP campus compound.

The received signal power at each test point was calculated using the link-budget equation (1), where P_{RX} is the received power, P_{TX} is the transmitter power, G_{TX} and G_{RX} are the transmitter and receiver antenna gains, respectively. $FSPL$ is the free-space path loss, and L_{MISC} represents estimated cable and connector losses [26].

$$P_{RX} = P_{TX} + G_{TX} + G_{RX} - FSPL - L_{MISC} \quad (1)$$

The free-space path loss, $FSPL$ was calculated according to (2), where f is the operating frequency in MHz and d is the distance between transmitter and receiver in km [26]:

$$FSPL(dB) = 32.45 + 20log_{10}(d) + 20log_{10}(f) \quad (2)$$

Miscellaneous losses, L_{MISC} were taken as the sum of transmitter and receiver side cable losses (3):

$$L_{MISC} = L_{TXCable} + L_{RXCable} \quad (3)$$

Finally, the link margin was computed as the difference between the calculated received power and the receiver sensitivity (4):

$$Link\ Margin = P_{RX} - P_{Sensitivity} \quad (4)$$

The calculations described above were performed using parameters extracted from the RFM95W module and the UG67 gateway datasheets and user manuals [27-29], as summarised in Table 6. Both the transmitter and the receiver operate at 915 MHz with a 125 kHz bandwidth. According to the datasheets, the transmitter exhibits a sensitivity of -140 dBm at SF12, and the receiver exhibits a sensitivity of -148 dBm at SF12. As the configuration used in this study is SF7, the sensitivity of both devices was conservatively estimated as -120 dBm. The sensor node employed an omnidirectional monopole antenna with a gain of 3 dBi, whereas the gateway was fitted with two 60 cm GA01 omnidirectional antennas with a gain of 5 dBi. The transmitter was configured in the standard RFO output mode at +14 dBm (maximum +20 dBm with PA_BOOST mode), and the gateway has a maximum transmit power of +27 dBm. Losses due to cables and connectors were conservatively assumed to be 3 dB at each device (transmitter and receiver) to avoid over-optimistic link-budget results.

https://doi.org/10.31436/iiumej.v27i1.3720

Table 6. Transmitter (sensor node) and receiver (gateway) parameters [27-29].

Parameter	Transmitter (RFM95W node)	Receiver (UG67 gateway)
Frequency	915 MHz	915 MHz
Bandwidth	125 kHz	125 kHz
Sensitivity	-120 dBm @ SF7	-120 dBm @ SF7
Antenna gain	3 dBi	5 dBi
Output power	+14 dBm	+27 dBm (max)
Cable Loss	3 dB	3 dB

Table 7 summarises the measured RSSI, the calculated free-space path loss, the theoretical received power (based on link budget analysis), and the fade margin for each test point. As shown in Table 7, path loss increases progressively, and the theoretical and measured signal levels decrease with increasing distance. Up to approximately 0.9 km, the measured RSSI closely follows the theoretical received power. In contrast, beyond 1.0 km, the measured values diverge more strongly, reflecting the effects of environmental obstructions and near-ground propagation losses not captured by the free-space model. The fade margin also decreases steadily with distance, indicating the diminishing link reliability at longer ranges. These results provide the quantitative basis for the RSSI-distance and SNR-distance relationships presented in Figures 29 and 30.

Table 7. Measured and calculated link-budget parameters at each test point.

No.	Distance (km)	Measured RSSI (dBm)	Free-Space Path Loss (dB)	Theoretical Received Power (dBm)	Fade Margin (dB)
1	0.1	-66.0	71.7	-55.7	64.3
2	0.2	-64.0	77.7	-61.7	58.3
3	0.3	-59.0	81.2	-65.2	54.8
4	0.4	-58.0	83.7	-67.7	52.3
5	0.5	-57.0	85.7	-69.7	50.3
6	0.6	-58.0	87.2	-71.2	48.8
7	0.7	-57.0	88.6	-72.6	47.4
8	0.8	-72.0	89.7	-73.7	46.3
9	0.9	-74.0	90.8	-74.8	45.2
10	1.0	-102.0	91.7	-75.7	44.3
11	1.1	-106.0	92.5	-76.5	43.5
12	1.2	-106.0	93.3	-77.3	42.7
13	1.3	-110.0	94.0	-78.0	42.0

Figure 29 presents the measured RSSI, compared with the theoretical received power derived from link-budget calculations at each test point. Both the measured and theoretical values exhibit a gradual decline with increasing distance, consistent with the expected increase in free-space path loss. Up to approximately 0.9 km, the measured RSSI broadly follows the theoretical curve, indicating that the link performance is primarily governed by free-space propagation. Beyond 1.0 km, however, the measured RSSI diverges sharply from the theoretical prediction, falling to -110 dBm at 1.3 km. This decline reflects additional attenuation from environmental obstructions, ground effects, and near-field losses not captured by the free-space model. Although the gateway's nominal sensitivity at SF12 is -140 dBm, using SF7 in this study yields a higher effective threshold, making successful demodulation more difficult at lower signal levels. The observed deviation between the theoretical and measured curves at longer ranges, therefore, illustrates the combined effects of non-line-of-sight conditions and reduced link margin, thereby defining the practical communication range limit for the tested configuration.

https://doi.org/10.31436/iiumej.v27i1.3720

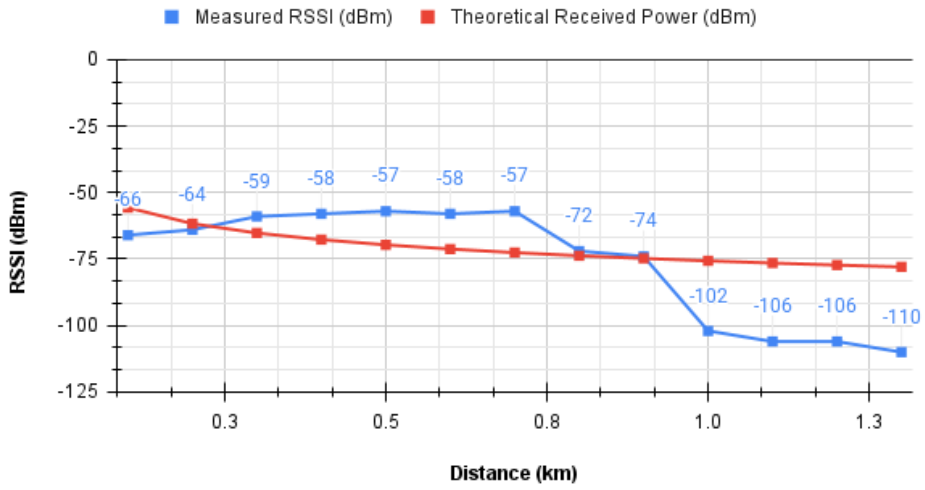

Figure 29. Measured RSSI and theoretical received power vs. distance.

Figure 30. SNR vs. Distance graph.

Figure 30 shows the variation of the Signal-to-Noise Ratio (SNR) with distance. SNR, which quantifies signal quality relative to background noise, exhibited small fluctuations at short ranges but showed a clear decline as distance increased. Beyond approximately 0.9 km, the SNR decreased sharply in parallel with the drop in RSSI, indicating that the link degradation was primarily caused by increased propagation loss rather than elevated noise levels. At the maximum test distance of 1.3 km, the low SNR values further limited the receiver's ability to reliably demodulate packets, demonstrating that maintaining adequate signal quality, not just signal power, is essential for long-range communication. This behaviour is consistent with observations reported in [30], in which both RSSI and SNR of LoRa-based links were found to decrease progressively with increasing range under field conditions.

The observed reduction in RSSI and SNR at longer distances was hypothesised to be influenced not only by environmental clutter but also by the relatively low installation heights of the transmitter and receiver antennas. In the initial configuration, the sensor node was positioned only 1 m above ground, whereas the gateway was mounted at 4 m, despite its elevation of 82 m. To examine whether antenna elevation could improve link performance, a supplementary test was conducted under the same conditions but with both antennas raised.

https://doi.org/10.31436/iiumej.v27i1.3720

A supplementary test was conducted at the same positions and at the same distance as shown in Figure 28. The repeated range test was conducted to evaluate the effect of raising the antennas of both the transmitter and the receiver on RSSI. During this test, both the gateway and the sensor were mounted on 8 m poles at the same points as in the previous test, as shown in Figure 31. The increase in the height of both the transmitter and the receiver yielded an RSSI value of -79 dBm at the 1.3km point, an improvement of 31 dB over the initial test configuration. This result is consistent with reports that increasing antenna height mitigates near-ground losses and improves line-of-sight [31]. Although LoRaWAN can achieve ranges of 15 km or more under ideal conditions, this study demonstrated a practical limit of 1.3 km within the campus environment, governed by antenna height, terrain clutter, and non-line-of-sight obstructions. The supplementary test, however, demonstrates that the developed system can be further improved by optimising the communication system design in future research.

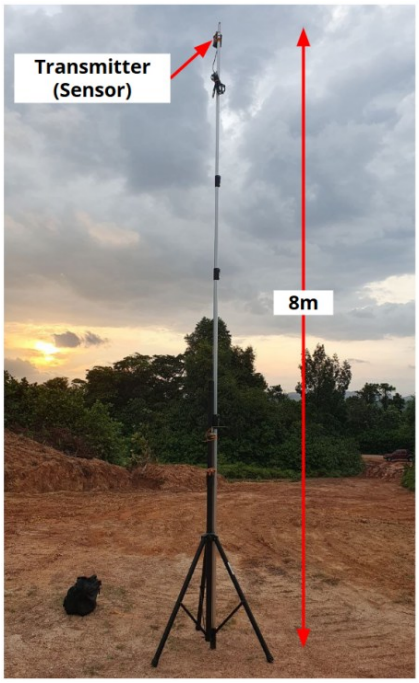

Figure 31. Transmitter applied to an increased height for a supplementary test.

6. CONCLUSION

The persistent challenge of Human-Elephant Conflict (HEC) in Malaysia has led to large-scale investment in electric fences, but maintaining these systems in remote areas remains costly and labour-intensive. This study demonstrated the feasibility of an integrated electric-fence monitoring system that combines a 10 kV voltage sensor, a short-circuit locator, and a gyroscope sensor, with a LoRaWAN-based data acquisition and a cloud-based monitoring dashboard. Field tests and simulation studies confirmed that the voltage sensor detected the electric fence voltage with 1 kV resolution. This demonstrates the feasibility of integrating high-voltage monitoring using the proposed method. The short-circuit locator sensor correctly identified fault locations using a 12 V reference supply. According to Sistem Pagar Elektrik Gajah (SPEG) technicians, fault-finding processes typically take 3-5 days to complete manually. The application of the short-circuit locator has the potential to reduce this fault-finding time to near-instantaneous, per-minute reporting. The gyroscope sensor can measure fence leaning with ≈99% accuracy, despite several design alterations made during testing, underscoring the need for proper orientation and a suitable test environment when using a gyroscope sensor. The developed data acquisition system using LoRaWAN link was also tested

over 30 days without data loss and achieved a practical range of 1.3km at SF7. A supplementary test showed that raising both the transmitter and receiver antennas further improved signal strength, indicating potential for additional range by underscoring the influence of antenna height and installation geometry on link performance.

These findings demonstrate that IoT-based monitoring can be adapted to rural electric-fence infrastructures to provide actionable, real-time data that has the potential to improve their overall reliability and system maintenance. Nevertheless, several limitations remain. The Hall-effect current-sensing approach for long-range fault localisation was only conceptually outlined and not yet validated. Range tests were conducted within a single campus environment and did not assess performance across different terrains or vegetation densities. Although the LoRaWAN link was stable for 30 days, longer-term reliability under field conditions and extreme weather remains to be established. At a 10m sensor node spacing, the cost for full coverage of a 4km energiser bay could reach RM 200,000, highlighting the need for scalable sensor placement strategies.

Future work will therefore focus on (i) implementing and experimentally validating the Hall-effect current-sensing approach for longer electric fence setups (kilometres-range), (ii) optimising antenna placement and LoRaWAN parameters to extend reliable coverage beyond 1.3 km, (iii) performing a detailed cost-benefit analysis for per-pole sensor deployment, and (iv) integrating predictive analytics to further reduce maintenance response time.

Overall, the study provides a quantitative foundation for designing and deploying remote electric fence monitoring systems and offers a practical pathway to enhance HEC mitigation by improving fence reliability and reducing maintenance effort.

ACKNOWLEDGEMENT

The authors gratefully acknowledge Universiti Teknologi PETRONAS (UTP), particularly the Civil & Environmental Engineering and Electrical and Electronics Engineering Departments, for their essential support in facilitating this research. Sincere appreciation is also extended to the primary stakeholder of this project, the Department of Wildlife and National Parks Peninsular Malaysia (PERHILITAN), for their invaluable collaboration and assistance throughout this study.

REFERENCES

[1] Sinha S. (2021). Visible and hidden costs of human-elephant conflict on smallholders in Peninsular Malaysia. PhD thesis. University of Nottingham.

[2] Xin LQ, Ghani SNAM, Rasudin NS, Ghafar NA, Abd Rashid NH, Ten DCY, Abdullah MT. (2024). Characterisation of human-wildlife conflict and casualties caused by wildlife attacks in Peninsular Malaysia. *IIUM Medical Journal Malaysia*, 23(1).

[3] Wildlife Conservation Society Malaysia. (2024). Elephants. [Online]. Available: https://malaysia.wcs.org/Wildlife/elephants.aspx (accessed: April 10, 2025).

[4] Saaban S, Othman N. (2006). Pelan Pengurusan Gajah Semenanjung Malaysia. Jabatan Perlindungan Hidupan Liar dan Taman Negara, Kuala Lumpur.

[5] Department of Wildlife and National Parks Peninsular Malaysia. (2015). Laporan tahunan PERHILITAN 2015. Department of Wildlife and National Parks Peninsular Malaysia, Kuala Lumpur.

[6] Jabatan PERHILITAN Semenanjung Malaysia. (2023). *Buku Panduan Spesifikasi Peralatan dan Penyelenggaraan Sistem Pagar Elektrik Gajah (SPEG)*. 1st ed. Kuala Lumpur, Malaysia: Kementerian Sumber Asli dan Kelestarian Alam.

[7] Scholes RJ, Mennell KG. (2008). Controlling the Distribution of Elephants. Witwatersrand University Press, Johannesburg.

[8] Van Eden M, Ellis E, Bruyere BL. (2016). The influence of human–elephant conflict on electric fence management and perception among different rural communities in Laikipia County, Kenya. *Human Dimensions of Wildlife*, 21:283-296.

[9] Fernando P, Ekanayaka SKK, Pastorini J. (2020). The elephant at the fence: almsman, panhandler, friend or foe? *European Journal of Wildlife Research*, 66:97.

[10] Sukumar R. (2003). The Living Elephants: Evolutionary Ecology, Behavior, and Conservation. Oxford University Press, New York.

[11] Gallagher Group Ltd. (n.d.). *Electric Fencing 101: Electric Fencing Systems Design, Installation & Maintenance.* [Online]. Available: https://am.gallagher.com/-/media/Bynder/Animal-Management/Document/All-GGL-Manuals/Electric-Fencing-101-Manual-NA-original.pdf (accessed: April 10, 2025).

[12] Tennakoon E, Madusanka C, De Zoysa K, Keppitiyagama C, Iyer V, Hewage K, Voigt T. (2015). Sensor-based breakage detection for electric fences. In: *2015 IEEE Sensors Applications Symposium (SAS)*; April 2015; pp.1-4. IEEE.

[13] Al-Bahadly I, Simpson R. (2019). Contactless electric fence fault detection system. In: *2019 IEEE International Instrumentation and Measurement Technology Conference (I2MTC)*; Auckland, New Zealand; 2019; pp.1-5. IEEE.

[14] Ali ASJ, Abdullah L, Musa M, Yunos MA, Ki NWW, Tukiran Z, Zainuddin MHAJ. (2020). Towards IoT-based notification system for agriculture electric fence. In: *2020 IEEE Student Conference on Research and Development (SCOReD)*; September 2020; pp.269-273. IEEE.

[15] Yunus MABY, Zainal MSB. (2023). IoT-based intelligent system for farm electric fence. *Progress in Engineering Application and Technology*, 4(2):274-286.

[16] Sendra S, García L, Lloret J, Bosch I, Vega-Rodríguez R. (2020). LoRaWAN network for fire monitoring in rural environments. Electronics, 9(3):531.

[17] Bouras C, Gkamas A, Kokkinos V, Papachristos N. (2022). Performance evaluation of monitoring IoT systems using LoRaWAN. *Telecommunication Systems*, 79:295-308.

[18] Khriji S, Günyeli ÖK, El Houssaini D, Kanoun O. (2022). Energy-efficient short-long range communication network combining LoRa and low-power radio for large-scale IoT applications. In: *2022 IEEE 9th International Conference on Computational Intelligence and Virtual Environments for Measurement Systems and Applications (CIVEMSA)*; Chemnitz, Germany; 2022; pp.1-6. IEEE.

[19] Senjaya A, Zulkifli FY. (2019). Low-cost continuous-wave radar system design for detection of human respiration rate. In: *2019 IEEE R10 Humanitarian Technology Conference (R10-HTC)*; Depok, West Java, Indonesia; 2019; pp.90-92. IEEE.

[20] Chen YH, Shen SC, Wu YK, Lee CY, Chen YJ. (2022). Design and testing of real-time sensing system used in predicting the leakage of subsea pipeline. Sensors, 22(18):6846.

[21] Fasasi MO. (2024). Comparative analysis of wired and wireless sensors in structural health monitoring. *Open Journal of Engineering Science*, 5(1):38-49.

[22] Oleksyn S, Tosetto L, Raoult V, Joyce KE, Williamson JE. (2021). Going batty: The challenges and opportunities of using drones to monitor the behaviour and habitat use of rays. *Drones*, 5(1):12.

[23] McGillan G. (2009). The design of an electric fence fault-finder. Master's thesis. Massey University, Albany, New Zealand.

[24] Datamars Ltd. (2023). 6 J, 12 J Unigizer™ User Guide, Issue 6. [Online]. Available: https://pel.co.nz/resource-hub/user-guides/406i-412i-unigizer-user-guide-enesptfrde (accessed: April 10, 2025).

[25] InvenSense. (2013). MPU-6000 / MPU-6050 Product Specification. Revision 3.4, Document Number PS-MPU-6000A-00.

[26] Campbell Scientific. (n.d.). *Application Note – The Link Budget and Fade Margin*. [Online]. Available: https://s.campbellsci.com/documents/us/technical-papers/link-budget.pdf (accessed: September 15, 2025).

[27] Milesight. (2025). *UG67 Datasheet.* [Online]. Available: https://resource.milesight.com/milesight/iot/document/ug67-datasheet-en.pdf (accessed: September 16, 2025).

[28] HopeRF. (n.d.). *RFM95W-V2.0 Datasheet.* [Online]. Available: https://cdn.sparkfun.com/assets/a/9/6/1/0/RFM95W-V2.0.pdf (accessed: September 17, 2025).

[29] MCCI. (2025). GA01 Gateway. [Online]. Available: https://store.mcci.com/products/milesight-ga01 (accessed: April 10, 2025).

[30] Križanović V, Grgić K, Spišić J, Žagar D. (2023). An advanced energy-efficient environmental monitoring in precision agriculture using LoRa-based wireless sensor networks. Sensors, 23(14):6332.

[31] Gutiérrez-Gómez A, Rangel V, Edwards RM, Davis JG, Aquino R, López-De la Cruz J, Geng Y. (2021). A propagation study of LoRA P2P links for IoT applications: The case of near-surface measurements over semitropical rivers. Sensors, 21(20):6872.